UNIVERSITY OF CALIFORNIA SAN DIEGO

Dynamical Modelling and Simulation of Field-Reversed Configuration (FRC) Plasmas for Feedback Control

A thesis submitted in partial satisfaction of the
requirements for the degree Master of Science

in

Engineering Sciences (Aerospace Engineering)

by

Georges Constantinos

Committee in charge:

Professor Alexey Arefiev, Chair
Professor Jorge Cortes
Professor William McEneaney

2021

The Thesis of Georges Constantinos is approved, and it is accepted in quality and form for publication on microfilm and electronically.

University of California San Diego

2021

TABLE OF CONTENTS

LIST OF SUPPLEMENTAL FILES

File 1. FRC Plasma MATLAB Solver, GeorgesConstantinosSupplemental FRC Plasma MATLAB Solver.rar

LIST OF SYMBOLS

$\vec{\xi}_{CEN}^{I}$	xyz-position of FRC plasma centroid in inertial frame
$\vec{\xi}_{p}^{B}$	xyz-position of FRC plasma differential volume element in body frame
r_{CEN}^{I}	Radial position of FRC plasma centroid in inertial frame
z_{CEN}^{I}	Axial position of FRC plasma centroid in inertial frame
$\vec{F}_{CEN}$	Net force on FRC plasma centroid in inertial frame
$\hat{e}_r$	Radial direction unit vector (cylindrical coordinate)
$\hat{e}_\phi$	Azimuthal/toroidal direction unit vector (cylindrical coordinate)
$\hat{e}_z$	Axial direction unit vector (cylindrical coordinate)
r_{C_i}	Radius of axial field coil 'i'
$z_{C_\mathrm{i}}^{I}$	Axial position of axial field coil 'i' in inertial frame
r_{PC_j}	Radius of plasma coil "j"
$z_{PC_j}^{B}$	Axial position of plasma coil "j" in plasma body frame
$\Delta r_C, \Delta z_C$	Axial field coil radial and axial thickness
$\Delta r_p, \Delta z_p$	Plasma coil radial and axial thickness
$\vec{f}_L$	Lorentz force density
p	FRC plasma pressure
$p_{\max}$	Maximum FRC plasma pressure (at the magnetic axis / O-point)
j_p	FRC plasma current density
j_θ	FRC plasma poloidal current density
j_ϕ	FRC plasma toroidal current density
J_p	FRC plasma current
J_{p_j}	Current through plasma coil "j"
m_p	FRC plasma mass
M_p	FRC plasma molar mass
n_p	FRC plasma number density
V_p	FRC plasma volume
B_θ	FRC plasma poloidal magnetic field strength
B_ϕ	FRC plasma toroidal magnetic field strength
ψ	FRC plasma poloidal magnetic flux
$\psi_{\max}$	FRC plasma maximum poloidal magnetic flux
g	FRC plasma toroidal magnetic flux
E	Separatrix elongation
R_{sep}	Separatrix radius at FRC midplane
Z_{sep}	Separatrix axial length
N_{sep}	Separatrix shape index
k	Elliptic Modulus
$K_{elliptic}$	Complete Elliptic Integral of 1st kind
$E_{elliptic}$	Complete Elliptic Integral of 2nd kind
N_C	Number of superconducting coils (axial field coils)
N_{PC}	Number of plasma coils (plasma body discretised into N_p coils).
M_{C_i,PC_j}	Mutual inductance between superconducting coil "i" and plasma coil "j"
$\vec{M}_{C,PC}$	Mutual inductance matrix ($N_C \times N_{PC}$) between SC coils and plasma coils
$\vec{M}_{C,C}$	Mutual inductance matrix ($N_C \times N_C$) between superconducting coils

$\vec{J}_{PC}$	Electric current through each of the N_{PC} plasma coils
$\vec{\Phi}_{C,PC}$	Magnetic flux through each superconducting coil due to FRC plasma
$\vec{\Phi}_{PC,C}$	Magnetic flux through FRC plasma due to all superconducting coils
$\vec{I}_{FC}$	Superconducting coil flux-conserving current
$\vec{I}_{C}$	Superconducting coil current
$B_{\mathrm{v}_r}, B_{\mathrm{v}_z}$	Radial and axial vacuum magnetic field (due to copper EM coils)
B_{C_r}, B_{C_z}	Radial and axial flux-conserving magnetic field (due to SC coils)
B_r^I, B_{z}^I	Total radial and axial magnetic field (due to all coil actuators) in inertial frame
$\vec{B}_{\mathrm{v}}^I$	Vacuum magnetic field (due to copper EM coils) in inertial frame
$\vec{B}_C^I$	Flux-conserving magnetic field (due to SC coils) in inertial frame
$\vec{B}^I$	Total magnetic field experienced by FRC plasma in inertial frame
μ_0	Vacuum permeability
N_A	Avogadro Number

LIST OF FIGURES

LIST OF TABLES

ACKNOWLEDGMENTS

Credit to supervisor Prof. Alexey Arefiev; thank you for your guidance on this body of work and for collaborating with the PSS team to better flesh out the activities of this thesis. You are a great teacher of plasma physics and make the subject matter highly enjoyable. It is a pleasure to work with you.

Credit to the Staff of Princeton Satellite Systems; namely, Dr. Charles Swanson for the consistent dialogue and assistance in understanding plasma dynamics and magnetic confinement of plasma as they pertain to the Princeton Field-Reversed Configuration. I especially thank Dr. Mike Paluszek and Dr. Stephanie Thomas for allowing me to conduct this brief body of work on your Direct Fusion Drive (DFD) program, for your expertise and for the supplemental material (solvers, internal documentation) that were most helpful.

ABSTRACT OF THE THESIS

Dynamical Modelling and Simulation of Field-Reversed Configuration (FRC) Plasmas for Feedback Control

by

Georges Constantinos

Master of Science in Engineering Sciences (Aerospace Engineering)

University of California San Diego, 2021

Professor Alexey Arefiev, Chair

The Direct Fusion Drive (DFD) is an advanced deep-space propulsion technology that utilises a field-reversed configuration (FRC) plasma core based on the PFRC-II laboratory test-bench located at the Princeton Plasma Physics Laboratory. A rigid-body model is derived for the translational kinematics of the FRC plasma and a numerical solver is developed in MATLAB to aid controller design and analysis for the FRC plasma centroid position. Two types of coil actuators are considered: superconducting flux-conservers and constant-current electromagnets. For constant-current coil actuators, the open-loop response of the FRC plasma

centroid position to radial perturbations is shown to exhibit standing radial oscillations about the origin at constant frequency (closed trajectories neither decaying nor growing), while for axial perturbations, the FRC plasma position is shown to be axially unstable (driven away from the origin axially). Results for flux-conservers are inconclusive, requiring further work. A well centred FRC plasma is critical for interpretation of diagnostics and analysis of experimental data, the rigid-body model and numerical solver devised are attempted first steps toward this goal.

Chapter 1. Introduction

Conventional deep-space travel involves transferring between orbits through a series of fuel-efficient manoeuvres such as Hohmann transfers and gravity assists (using planetary bodies to further accelerate spacecraft, reaching deeper into space). This means deep-space travel typically involves detours and numerous manoeuvres prior to arriving at the destination. For background, ion thrusters produce on the order of milli-newtons of thrust (long duration burns) and have specific impulse in the range <5000s (low thrust, high Isp), while chemical rockets produce vacuum thrust on the order of kilo-newtons (strictly short duration burns) and have specific impulse of roughly <500s (high thrust, low Isp).

Princeton Satellite Systems (PSS) and the Princeton Plasma Physics Laboratory (PPPL) are engaged in the development of a new deep-space propulsion technology known as the Direct Fusion Drive (DFD), funded primarily by NASA and ARPA-E. This advanced propulsion concept employs the use of a FRC plasma core (explained next) that is confined magnetically using coils (+7T). The engine class is thermo-nuclear, producing on the order of 5-10 N of thrust per MW and a specific impulse of 10000-20000s (high thrust, high Isp). The DFD is intended for deep-space and interplanetary missions with preliminary studies exploring *direct transit* to Jupiter within 1 year and to outer edges of the Solar System, Pluto, within 5 years (for a 1-2 MW engine) [1]. The electrical power generated by this drive provides a drastic change in power budget available for scientific or commercial payloads, on the order of 1MW, unseen to date. It is simply posed as a game changing technology in the areas of both energy generation and space flight.

1.1 Overview of Field-Reversed Configuration (FRC) Plasmas

A field-reversed configuration (FRC) is a type of plasma that exhibits a compact toroid structure, as shown in Figure 1. FRC plasmas are magnetically confined to this shape purely

by a poloidal magnetic field (black contours in Figure 1, shown inside the plasma) which is produced by a toroidal current that has been induced in the plasma (indicated by the red arrow). Also shown, FRC plasma is embedded within coils that produce an external confinement field for sustainment of the FRC plasma and keeping it in place.

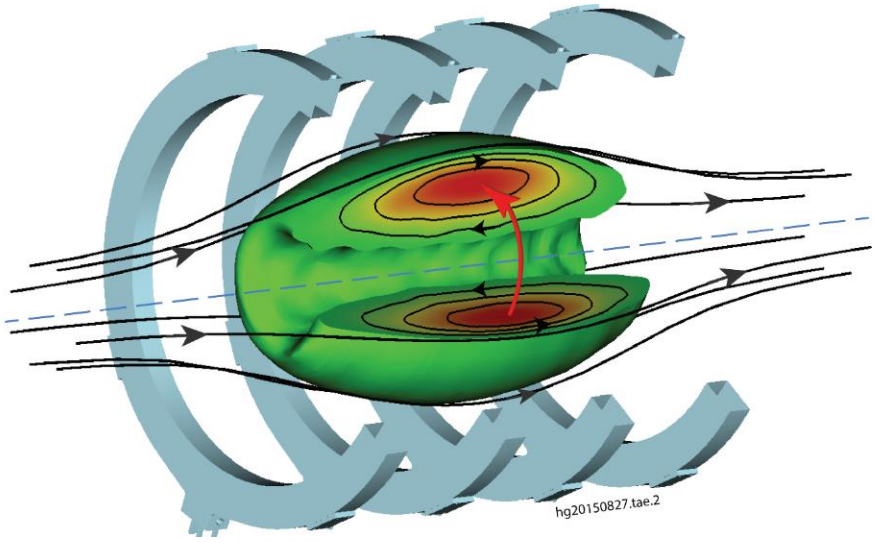

Figure 1. Field-Reversed Configuration (FRC) Plasma embedded in Coil Actuators [2]

Unlike tokamak configurations shown in Figure 2, FRCs do not have a centre structure running through the plasma (no *inner poloidal field coil*) nor do they have *toroidal field coils*. FRCs are thus a considerably simpler device.

This area of research, explored initially in the late 1950's suffered plasma stability issues for almost two decades (unable to maintain a steady-state plasma/equilibrium). Breakthroughs were made by Soviet researchers in the 1980's in overcoming unstable FRC plasma dynamic modes [3], eventually leading to FRCs regaining popularity in thermo-nuclear fusion devices. The key attraction of FRCs is extremely high-β (x20 greater than tokamaks) which is one metric used for reactor cost-benefit/return on investment, x10 greater confinement than tokamaks, significantly lower form-factor and simpler machine configuration (cylindrical vacuum vessel, reduced magnet complexity), and exhibiting x5 higher plasma density [4].

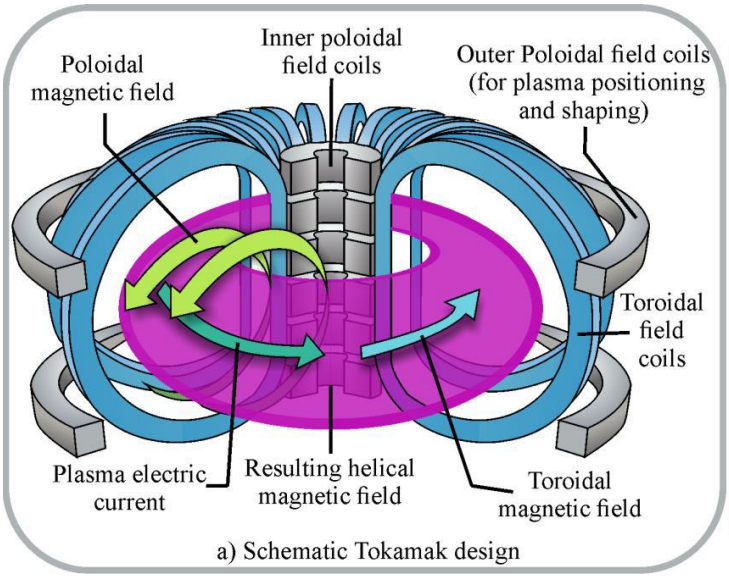

Figure 2. Tokamak Magnetic Field Configuration [5]

1.2 Direct Fusion Drive (DFD) Experimental Setup

The DFD employs the Princeton Field-Reversed Configuration (PFRC) a fusion energy core invented by Dr. Samuel Cohen at PPPL, employing the use of a FRC plasma, where high energy particles are extracted from the plasma core via the scrape off layer (SOL) and expelled out a magnetic nozzle generating high thrust.

The DFD experimental setup is located at the PPPL and is shown in Figure 3. Key features of the propulsion system and FRC plasma core are defined in Section 1.2.1.

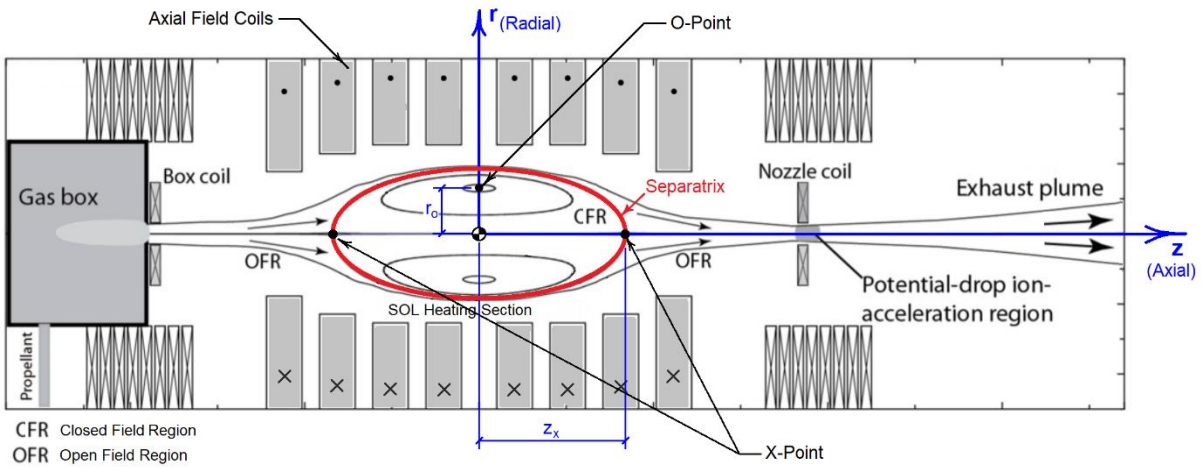

Figure 3. Direct Fusion Drive (DFD) Experimental Setup, Cross-Section (adapted from [4])

1.2.1 FRC Plasma Definitions

Magnetic Separatrix: the boundary highlighted red in Figure 3 that separates *closed* magnetic flux surfaces from *open* magnetic flux surfaces, labelled as CFR and OFR. The separatrix defines the Last Closed Flux Surface (LCFS) since all magnetic flux surfaces outside the separatrix are unconfined. The dashed-line in Figure 4 provides another illustration of the separatrix with magnetic flux contours. The magnetic field strength at the separatrix is 0T.

O-Point (or Magnetic Axis): is a 'magnetic null' within the FRCs defined by a radial position (r_o) relative to the FRC centroid, as identified in Figure 3. It is the innermost magnetic surface existing as a circular-line in the transverse plane, along which it is a magnetic null. The magnetic field lines within the FRC are reversed when crossing the O-point radially, as shown in Figure 4 (i.e. magnetic field lines below the O-point travel in opposite direction to field lines above the O-point). This reversal gives rise to the name "Field-Reversed" Configuration [3].

X-Point: point at which the FRC's poloidal magnetic field is zero ($B_{poloidal} = 0\text{T}$) and is defined by an axial position (z_x) relative the FRC centroid, as identified in Figure 3. The X-point also intersects the Separatrix.

Separatrix Elongation ($E = Z_{sep}/2R_{sep}$): the length-to-diameter ratio of the separatrix. *Oblate* FRCs have E < 1, and *Prolate* FRCs have E > 1 [3].

Axial Field Coil: coil actuators responsible for magnetically confining the FRC plasma (performing stabilisation and/or control) and keeping plasma away from the vacuum vessel walls. Axisymmetric coils are currently employed as shown in Figure 3. Refer Section 1.2.2.2.a.i. for further detail.

Nozzle Coil: coil actuators that act as *magnetic mirrors* to create strong restoring forces in the axial direction at the machine ends. They effectively reflect the FRC plasma back toward

the origin. The nozzle coil is responsible for producing a sufficiently deep “magnetic well” [6] about the origin to aid the stability of magnetically confined plasma.

Scrape Off Layer (SOL): is the outer edge of the plasma. The SOL is a region of plasma characterised by *open* field lines i.e. it resides just outside the separatrix/LCFS. Its purpose is to the online removal of fusion by-products from the plasma core redirected for useful thrust whilst in operation. The SOL allows control over the build-up of fusion products and removes impurities in the plasma.

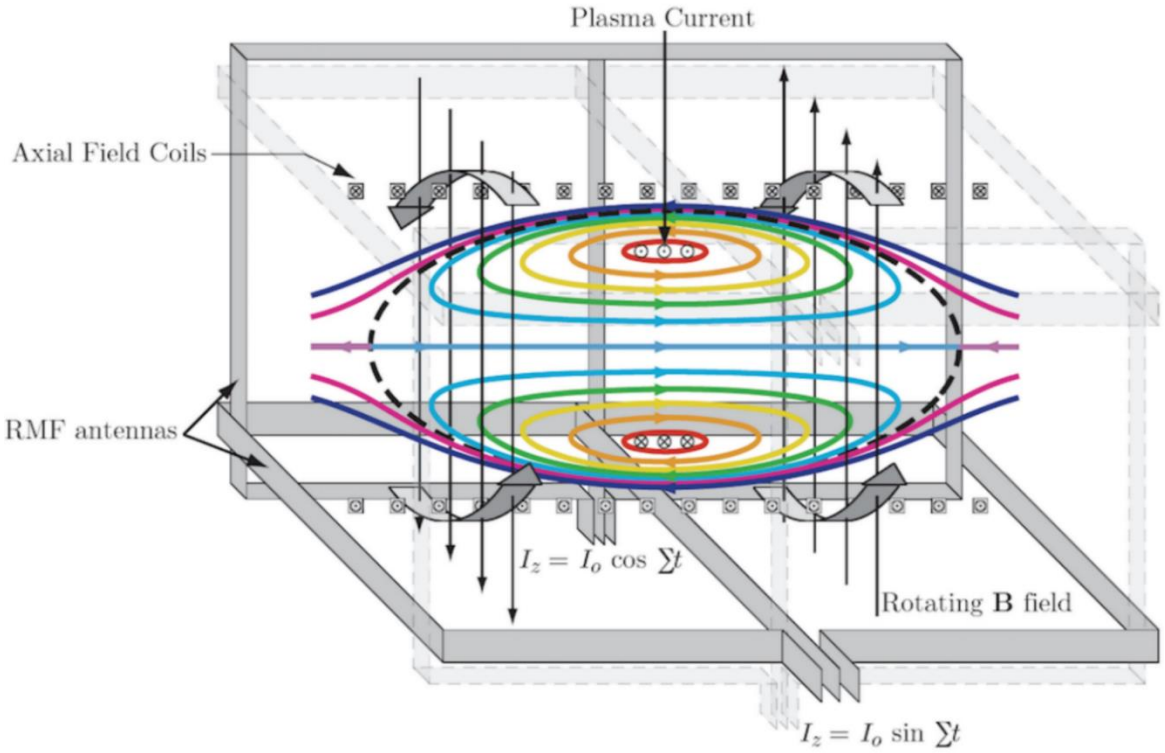

Figure 4. Field-Reversed Configuration (FRC) Plasma Magnetic Flux Surfaces [4]

1.2.2 DFD Actuators

1.2.2.1 Coil Actuator Types

Two types of coil actuators are employed on DFD and share the responsibility of magnetically confining the FRC plasma core, these are:

a) *Powered Coils:* These are electromagnetic (EM) copper coil actuators. EM coils have active control currents that produce a magnetic field based on coil geometry.

b) *Unpowered, Flux-Conserving Coils:* These are superconducting (SC) coil actuators. SC coils do not have active control currents (as with EM coils), instead flux-conserving currents are induced in the coil to counteract externally applied magnetic flux (such as flux introduced by existence of plasma / conducting fluid). Currents are induced at speed of light (assumed instantaneous, no time delay).

1.2.2.2 Coil Actuator Geometry

Two geometries/configurations are investigated for coil actuators on DFD:

a) *Axisymmetric Coils:* for stabilisation/control of plasma axisymmetric modes (m=0). There are two axisymmetric coil arrangements considered for DFD *axial field coils*:

   i. *Ellipsoidal Solenoid (Space Configuration):* coil radii have an ellipsoidal profile per Figure 3. This provides a significant mass and size reduction in magnet hardware relative to a uniform solenoid. Ideal for spacecraft as magnet hardware constitutes almost a third of the total DFD mass [4].

   ii. *Uniform Solenoid (Terrestrial Configuration):* coil radii are equal, as shown in Figure 1. Ideal for economic scaling due to ease of manufacture and cost savings (reduced complexity) relative to ellipsoidal solenoid.

b) *Saddle Coils:* for stabilisation/control of non-axisymmetric modes (example: FRC plasma tilt mode (m=1, n=1), radial elongation mode (m=2)). Sometimes referred to as *trim coils*.

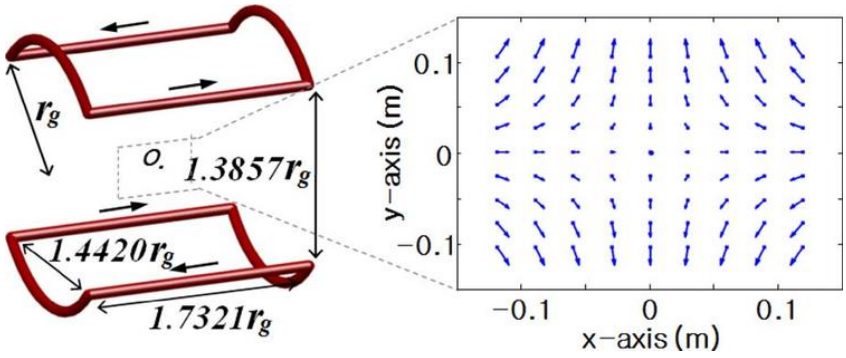

Figure 5. Saddle Coil Actuator [7]

N.B. The actuator coils would also perform as a sensor, that is for pickup rather than for actuation, used for feedback control. For example, plasma centroid position may be estimated by inference from flux-conserving currents along superconducting coils.

1.3 Commercial Background

An overview of external stakeholders for this project are listed in Table 1:

Table 1. Direct Fusion Drive (DFD) External Stakeholders

Organisation	Name	Title
Princeton Satellite Systems (PSS)	Dr. Michael Paluszek	PSS President
	Ms. Stephanie Thomas	PSS Vice President DFD Principal Investigator
	Dr. Charles Swanson	Chief Scientist
Princeton Plasma Physics Lab (PPPL)	Prof. Samuel A. Cohen	Inventor of the PFRC reactor core employed on DFD

This thesis (MAE299 research units) is funded by SPACEBUS Pty. Ltd. for purposes of training. The author had become acquainted with PSS through SPACE INDUSTRIES Pty. Ltd. who are developing technologies to extract helium-3 from lunar regolith. PSS has interest in the rare isotope helium-3 as an advanced fuel for the DFD and PFRC.

Chapter 2. Criteria for Verification of Numerical Results

Table 2 outlines expected responses for FRC centroid position as theorised in [8] and [9], and based on experimental data/observations on the PFRC per consultation with PSS. These form criteria against which numerical results produced by this thesis will be verified qualitatively for the purpose of developing a tool for control design and systems analysis.

Table 2. Qualitative Criteria for Verification of Numerical Results

Case	Perturbation	Actuator Coil	Expected Plasma Response
1	Radial perturbation to FRC centroid position	- Copper Electromagnet - Axisymmetric Coil - Constant Current	*Stable* or *bounded* open-loop response in axial and radial position (for $B_{\mathrm{v}_z} < 0$)
2	Axal perturbation to FRC centroid position	- Copper Electromagnet - Axisymmetric Coil - Constant Current	*Unstable* or *unbounded* open-loop response in axial position (for $B_{\mathrm{v}_z} < 0$)
3	3DOF perturbation to FRC centroid position	- Superconductor - Axisymmetric Coil - Flux-conserving Current	Unknown. Expecting *stable*/bounded radial and axial position. Expecting plasma position to be "locked" relative to SC coils (plasma flux completely counteracted by SC coils, hence resisting changes in FRC position)

N.B. Position perturbations are relative to the origin.

Chapter 3. Dynamical System Modelling of FRC Plasmas

3.1 Reference Frame Definitions

Let the Inertial Frame and FRC Plasma Body Frame be Cartesian Coordinate Systems defined in Figure 6. The Inertial Frame, labelled {I}, is located at the origin of the PFRC machine (see Figure 3). The Plasma Body Frame, labelled {B}, has origin at plasma centroid.

The poloidal coordinate (θ), also defined in Figure 6, resides within the plasma x-z body plane (r-z plane in cylindrical coordinates), and the toroidal coordinate (ζ) resides within the plasma x-y body plane (ϕ in cylindrical coordinates).

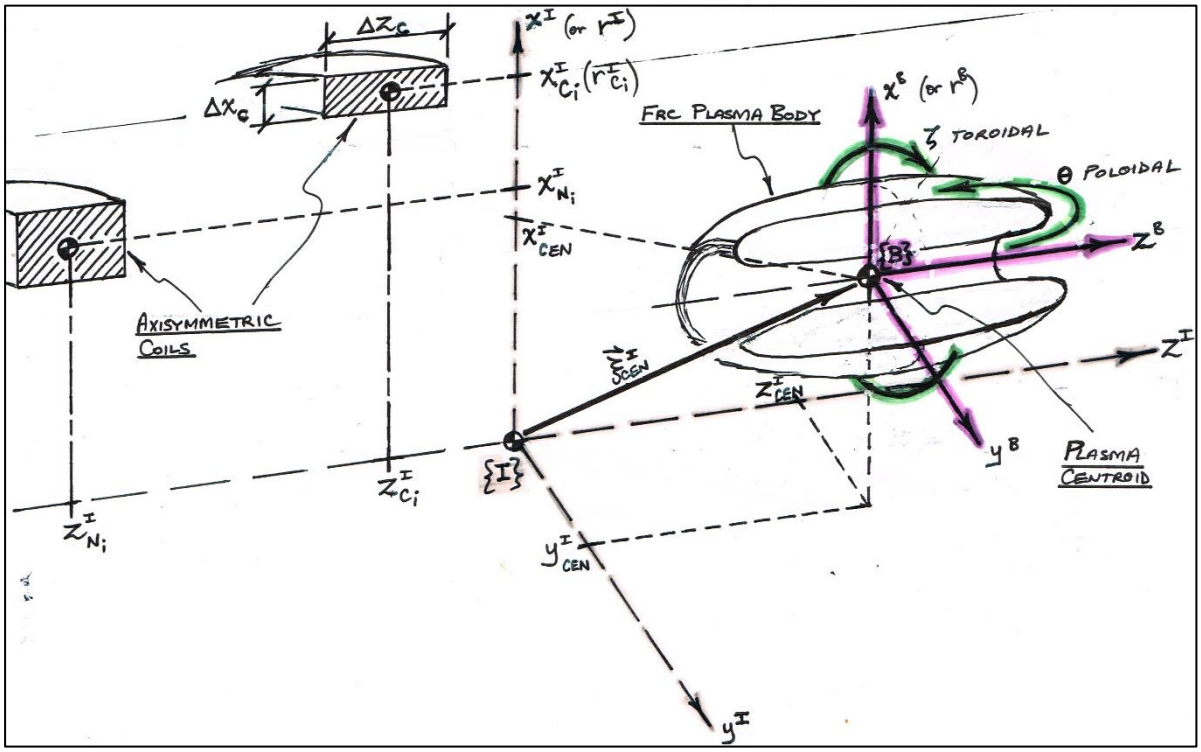

Figure 6. Definition of Inertial and Plasma Body Frames (Cartesian Coordinates)

From Figure 6:

{I} is inertial frame of reference.

{B} is plasma body frame of reference.

(θ, ζ) are poloidal and toroidal coordinates defined in the plasma body frame.

$\vec{\xi}^{I}_{\mathrm{CEN}} = [x^{I}_{\mathrm{CEN}}\ \ y^{I}_{\mathrm{CEN}}\ \ z^{I}_{\mathrm{CEN}}]$ is FRC plasma centroid position in the inertial frame.

$\left(x^{I}_{C_i}, z^{I}_{C_i}\right)$ is the i[th] axisymmetric coil cross-section centroid in the Inertial frame.

$(\Delta x_C, \Delta z_C)$ is the coil's radial and axial thickness.

3.2 Modelling Electromagnetic Force on Plasma Element

Using Magnetohydrodynamic (MHD) theory, the FRC plasma is modelled as an electrically conducting fluid consisting of charged particles (specifically two species, electrons and ions, differing significantly in mass and charge) moving through an external magnetic field. A comparison of plasma modelling techniques is provided in Figure 7 to illustrate the differences in complexity captured. This thesis focuses on *"Plasma as a fluid"*.

	Magnetohydrodynamics	Two Fluids	Gyrokinetics	Kinetics	Everything
Description	The plasma is one continuous fluid - ions have all the mass, but electron carry all the current.	Break the ions & electrons into two continuous, mingling fluids.	Only track superparticles' straight motion - and ignore the corkscrewing.	Assign particles a speed and location based on a distribution. Track super particles through space.	Track every particle, at all times.
Strengthens	Easily solved.	Simple bulk effects like drift waves & reconnection can be understood.	Captures most of kinetic model, but much easier to solve - can model an entire Tokamak.	Many things captured, can get powerful results like the linear velocity-space instabilities.	Most accurate model possible.
Weakness	Most things not captured: most plasma waves, leakage, kinetic instabilities, structures etc.	Many things not captured: plasma instabilities, large effects & non-equilibrium effects. Assumes bell curves.	Non-physical behavior over long times: resonances & adiabatic invariants can be lost.	Tough to solve: hard to apply to full-size reactors. Loses some effects: like plasma microdensity and collective thomson scattering.	Typically impossible to solve.
Mathematics	Navier-stokes, Lorentz force, Maxwells' equations.	Navier-stokes, Lorentz force, Maxwells' equations.	Vlasov-Maxwell Expansion Equation	Vlasov-Maxwell Equation	Klimontovich Model

Plasma as a fluid (Chalkboard) — Plasma as a gas (Computer Required)

Simplicity — Detail

Figure 7. Comparison Chart for Modelling Plasma [10]

The FRC plasma is assumed to be a continuous charge distribution in motion (charge density ρ moving with velocity v_q). Electromagnetic forces acting on a differential element of FRC plasma due to external electric field $\vec{E}$ and magnetic field $\vec{B}$ are given by the Lorentz force-density $\vec{f}_L$ (per unit volume) as expressed in Equation (1) and illustrated in Figure 8.

$$\vec{f}_L = \rho\left(\vec{E} + \vec{v}_q \times \vec{B}\right) = \rho\vec{E} + \left(\rho\vec{v}_q \times \vec{B}\right) = \vec{f}_E + \vec{f}_M \qquad (1)$$

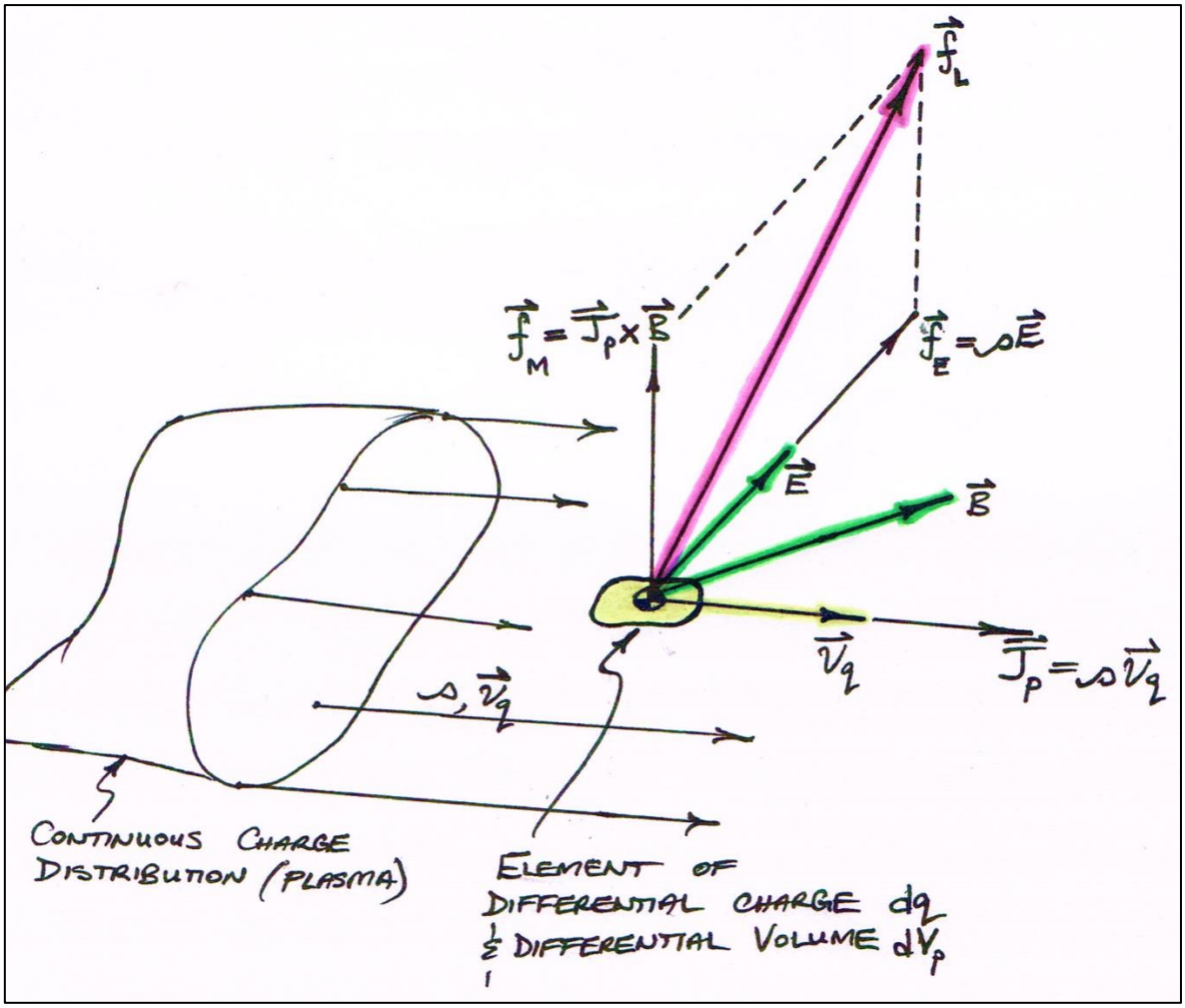

Figure 8. Electromagnetic Forces Acting on a Plasma Element of (dq, dV_p)

The plasma current density $\vec{J}_p$ associated with the moving charge distribution is:

$$\vec{J}_p = \rho\vec{v}_q \tag{2}$$

Given no electric fields act on the plasma ($\vec{E} = \vec{0}$) and the plasma current from Equation (2), the net electromagnetic force $\vec{F}_L$ acting on the FRC plasma is found by integration of the force density in Equation (1) over the charge distribution (plasma volume V_p), as follows:

$$\vec{F}_L = \int f_L \, dV_p = \int \vec{J}_p \times \vec{B} \, dV_p \tag{3}$$

3.3 Axisymmetric Assumption

The FRC plasma is assumed to be axisymmetric about the z-axis per cylindrical coordinates in Figure 28. Thus, the spatial derivative with respect to this dimension:

$$\frac{\partial}{\partial \phi} = 0 \tag{4}$$

For example, FRC plasma toroidal current is invariant toroidally, thus $\frac{\partial \vec{J}_p}{\partial \phi} = 0$.

3.4 (MHD Constraint 1) Momentum Equation for Plasma in Equilibrium

The force balance for a FRC plasma, using EM force derived in Equation (3), is:

$$m_p \frac{d\dot{\xi}_{CEN}}{dt} = \int \vec{J}_p \times \vec{B}_p - \nabla p \; dV_p \tag{5}$$

Where m_p is plasma mass, ξ_{CEN} is plasma centroid position in the inertial frame, $\vec{J}_p$ is plasma current density, $\vec{B}_p$ is magnetic field acting on the plasma, p is plasma pressure and V_p is plasma volume.

The condition for equilibrium of the FRC plasma centroid position due to p is $d\dot{\xi}/dt = 0$ (given the FRC exhibits "macro-equilibrium" per [11]), resulting in the equilibrium equation:

$$\nabla p = \vec{J}_p \times \vec{B}_p \tag{6}$$

Thus, the magnetic forces acting within the plasma (Lorentz force $\vec{f}_L = \vec{J}_p \times \vec{B}_p$) must balance forces due to the plasma pressure ∇p. Further, by scalar triple product:

$$\nabla p = \vec{J}_p \times \vec{B}_p \quad \Longrightarrow \quad \begin{matrix} \vec{B}_p \cdot \nabla p = \vec{B}_p \cdot \left(\vec{J}_p \times \vec{B}_p\right) = \vec{J}_p \cdot \left(\vec{B}_p \times \vec{B}_p\right) = 0 \\ \vec{J}_p \cdot \nabla p = \vec{J}_p \cdot \left(\vec{J}_p \times \vec{B}_p\right) = \vec{B}_p \cdot \left(\vec{J}_p \times \vec{J}_p\right) = 0 \end{matrix} \tag{7}$$

Thus, magnetic field ($\vec{B}_p$) and plasma current ($\vec{J}_p$) are perpendicular to pressure gradient

$$\vec{B}_p \cdot \nabla p = 0 \quad \Longrightarrow \quad \text{plasma pressure is constant along magnetic field lines}$$

Thus from Equation (7), to satisfy equilibrium conditions for FRC plasma centroid position, both the magnetic field ($\vec{B}_p$) and plasma current ($\vec{J}_\phi$) must lie on magnetic flux surfaces, as illustrated in Figure 9 for an isosurface of FRC plasma pressure (in the shape of a toroid). This is a similar situation for tokamak plasmas per pg.7 of [12].

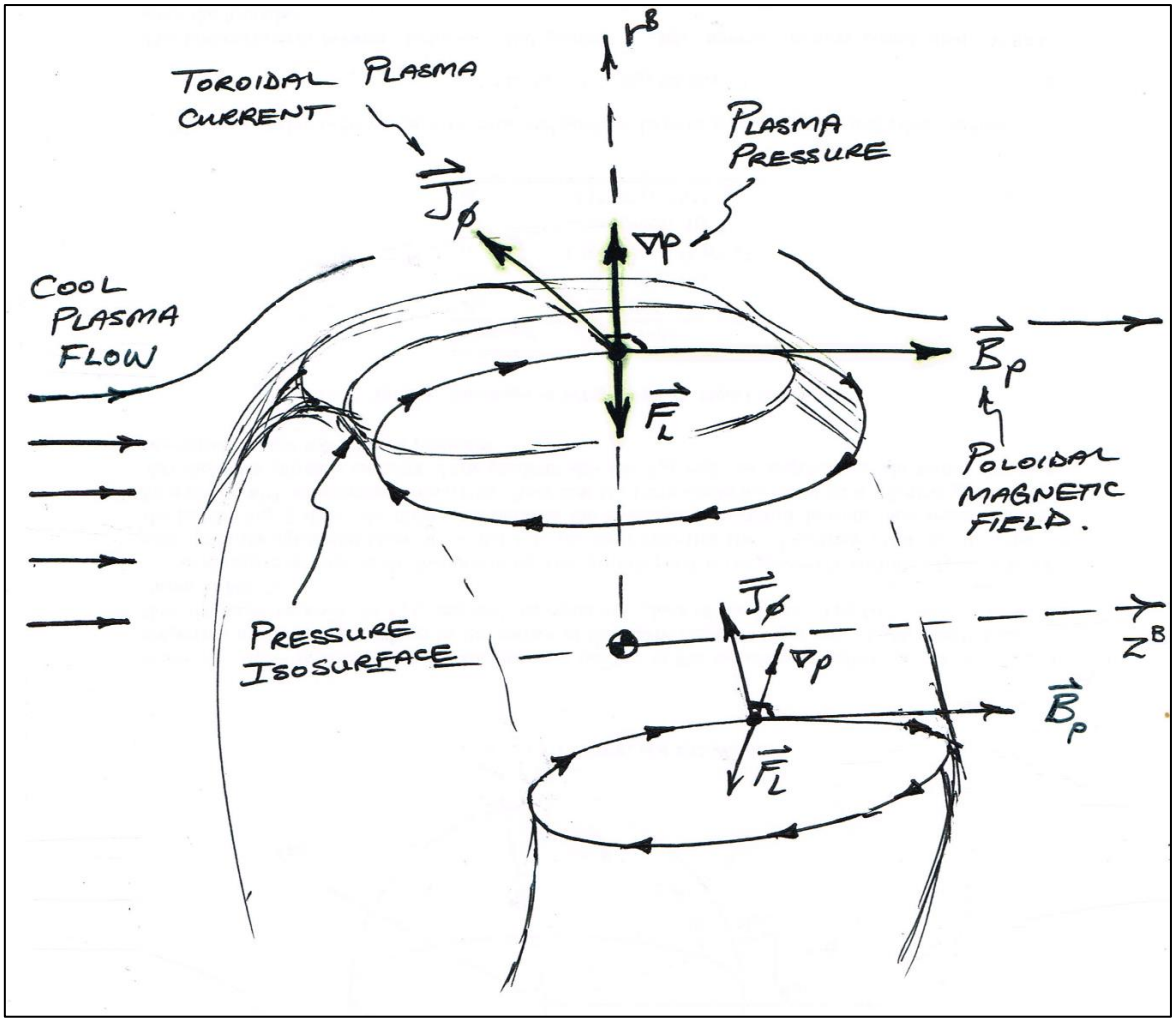

Figure 9. FRC Plasma Isosurface of Pressure and Force Balance

In summary, per Figure 9, the toroidal electric current generated in the FRC plasma produces a poloidal magnetic field (due to Ampere's law $\nabla \times B = \mu_0 J$). The poloidal magnetic field and toroidal current generate an inward Lorentz force ($\vec{F}_L$), and as previously established, this must be inward to counteract the outward magnetic pressure force per Equation (6).

3.5 (MHD Constraint 2) Gauss's Law for Magnetism

The FRC plasma does not exhibit magnetic field sources or sinks other than moving electric charges (the total plasma magnetic flux Φ_p penetrating a closed surface is zero), thus, Gauss's Law for Magnetism holds:

$$\Phi_p = \nabla \cdot \vec{B}_p = 0 \tag{8}$$

Since $\vec{B}_p$ is divergence-free, Poincare's Theorem dictates there must exist a magnetic vector potential $\vec{A}$ as follows (expressed in cylindrical coordinates per Equation (67)):

$$\nabla \cdot \vec{B}_p = 0 \quad \Longrightarrow \quad \exists \vec{A} \quad \text{s.t.} \quad \vec{B}_p = \nabla \times \vec{A} \tag{9}$$

Given the FRC plasma is assumed axisymmetric per Equation (4) $\frac{\partial A_\phi}{\partial \phi} = \frac{\partial A_r}{\partial \phi} = 0$, and curl in cylindrical coordinates is given per Equation (69), the net magnetic field in cylindrical coordinates is:

$$\vec{B}_p = \nabla \times \vec{A} = -\frac{\partial A_\phi}{\partial z}\hat{e}_r + \left(\frac{\partial A_r}{\partial z} - \frac{\partial A_z}{\partial r}\right)\hat{e}_\phi + \frac{1}{r}\frac{\partial}{\partial r}\left(rA_\phi\right)\hat{e}_z \tag{10}$$

3.5.1 Poloidal Magnetic Field

The poloidal component (defined in Section 3.1) of the magnetic field in Equation (10):

$$\vec{B}_\theta = -\frac{\partial A_\phi}{\partial z}\hat{e}_r + \frac{1}{r}\frac{\partial}{\partial r}\left(rA_\phi\right)\hat{e}_z \tag{11}$$

$$= -\frac{1}{r}\frac{\partial}{\partial z}\left(rA_\phi\right)\hat{e}_r + \frac{1}{r}\frac{\partial}{\partial r}\left(rA_\phi\right)\hat{e}_z$$

Poloidal magnetic field $\vec{B}_\theta$ is shown to only be a function of toroidal potential A_ϕ (independent of A_r, A_z). Let the poloidal magnetic *flux* be defined as follows:

$$\psi \coloneqq -rA_\phi \tag{12}$$

Recalling the following relationship for cylindrical coordinate systems:

$$\nabla\phi = \frac{1}{r}\hat{e}_\phi \tag{13}$$

Substituting Equation (12) and (13) into Equation (11), gives poloidal magnetic field:

$$\vec{B}_\theta = -\frac{1}{r}\frac{\partial\psi}{\partial z}\hat{e}_r + \frac{1}{r}\frac{\partial\psi}{\partial r}\hat{e}_z$$

$$= \frac{1}{r}\frac{\partial\psi}{\partial z}\left(\hat{e}_z \times \hat{e}_\phi\right) + \frac{1}{r}\frac{\partial\psi}{\partial r}\left(\hat{e}_r \times \hat{e}_\phi\right)$$

$$= \left(\frac{1}{r}\frac{\partial\psi}{\partial r}\hat{e}_r + \frac{1}{r}\frac{\partial\psi}{\partial z}\hat{e}_z\right) \times \hat{e}_\phi$$

$$= \left(\frac{\partial\psi}{\partial r}\hat{e}_r + \frac{\partial\psi}{\partial z}\hat{e}_z\right) \times \frac{1}{r}\hat{e}_\phi$$

$$= \nabla\psi \times \nabla\phi \tag{14}$$

Where: $\nabla\psi = \left[\frac{\partial\psi}{\partial r},\ 0,\ \frac{\partial\psi}{\partial z}\right]^{\mathrm{T}}$ per Equation (4), is the poloidal magnetic flux gradient. Equation (14) and poloidal flux contours are illustrated in Figure 10 in the plasma body frame**.**

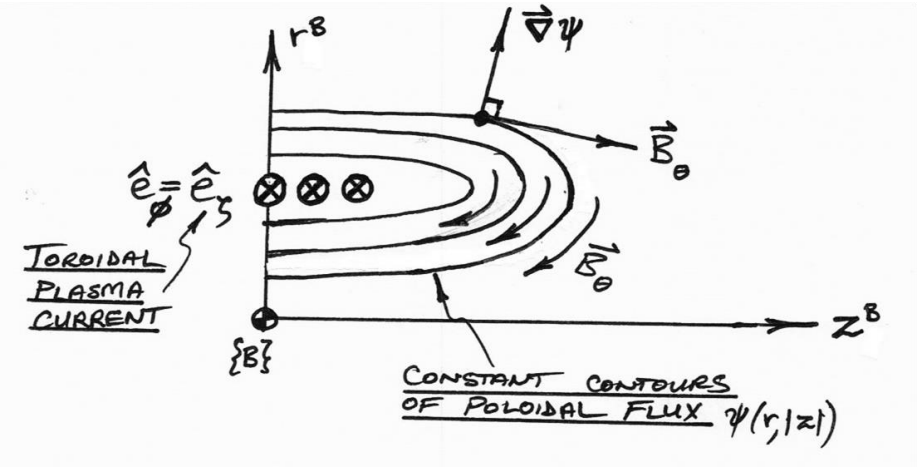

Figure 10. Poloidal Magnetic Flux Contours in the Plasma Body Frame (r-z plane)

3.5.2 Toroidal Magnetic Field

The toroidal component (defined in Section 3.1) of the magnetic field in Equation (10):

$$\vec{B}_\phi = \left(\frac{\partial A_r}{\partial z} - \frac{\partial A_z}{\partial r}\right)\hat{e}_\phi = B_\phi \hat{e}_\phi = \left(rB_\phi\right)\frac{1}{r}\hat{e}_\phi \tag{15}$$

Let the toroidal magnetic *flux* be defined as follows:

$$g \coloneqq rB_\phi \tag{16}$$

Substituting Equation (13) and (16) into Equation (15), gives toroidal magnetic field:

$$\vec{B}_\phi = g\nabla\phi \tag{17}$$

3.5.3 Total Plasma Magnetic Field

The total magnetic field in Equation (10) is re-expressed using Equations (15) and (14):

$$\vec{B}_p = \vec{B}_\theta + \vec{B}_\phi = \nabla\psi \times \nabla\phi + g\nabla\phi \tag{18}$$

3.6 (MHD Constraint 3) Ampere's Circuit Law

The magnetic field associated with plasma current ($\vec{J}_p$) and changes in electric field (E) is expressed using Ampere's Law:

$$\nabla \times \vec{B}_p \;=\; \mu_0\left(\vec{J}_p + \varepsilon_0\frac{\partial E}{\partial t}\right) \tag{19}$$

Substituting Equation (18) and given $E = 0$, the plasma current density is expressed as:

$$\mu_0\vec{J}_p = \nabla \times \vec{B}_p$$

$$= \nabla \times \left(\vec{B}_\theta + \vec{B}_\phi\right) \tag{20}$$

$$= \nabla \times \vec{B}_\theta + \nabla \times \vec{B}_\phi$$

3.6.1 Poloidal Current Density

Expanding the current density term responsible for toroidal flux ($\vec{B}_\phi$) in Equation (20):

$$\nabla \times \vec{B}_\phi = \nabla \times (g\nabla\phi)$$

$$= g\nabla \times \nabla\phi + \nabla g \times \nabla\phi \quad \text{(product rule for multiplication by scalar)} \qquad (21)$$

Since $\nabla \times \nabla\phi = \vec{0}$, second derivative is zero, poloidal plasma current density is thus:

$$\vec{J}_\theta = \frac{1}{\mu_0}\nabla g \times \nabla\phi \qquad (22)$$

3.6.2 Toroidal Current Density

Expanding the current density term responsible for poloidal flux ($\vec{B}_\theta$) in Equation (20):

$$\nabla \times \vec{B}_\theta = \nabla \times (\nabla\psi \times \nabla\phi)$$

$$= \nabla\psi(\nabla \cdot \nabla\phi) - \nabla\phi(\nabla \cdot \nabla\psi) + (\nabla\phi \cdot \nabla)\nabla\psi - (\nabla\psi \cdot \nabla)\nabla\phi$$

$$= -\nabla\phi(\nabla \cdot \nabla\psi) \qquad (23)$$

Since:

$(\nabla \cdot \nabla\phi) = 0$, divergence of field $\hat{e}_\phi$ is zero.

$(\nabla\phi \cdot \nabla) = 0$, $\frac{\partial}{\partial\phi} = 0$ per Section 3.3 and Equation (13).

$(\nabla\psi \cdot \nabla)\nabla\phi = \vec{0}$, poloidal flux ($\psi$) is expressed in r-z-coordinates, thus no derivative in toroidal direction.

The toroidal plasma current density is thus:

$$\vec{J}_{\phi} = -\frac{1}{\mu_0}\nabla\phi(\nabla \cdot \nabla\psi) \tag{24}$$

Equation (24) shows the electric current responsible for producing the poloidal magnetic field ($\vec{B}_{\theta}$) is purely toroidal ($\hat{e}_{\phi}$), consistent with assumptions held in Section 3.7 for FRC plasmas and illustrated in Figure 4.

3.6.3 Total Plasma Current Density

The total plasma current density is given by substituting Equations (22) and (24) into Equation (20):

$$\mu_0\vec{J}_p = -\nabla\phi(\nabla \cdot \nabla\psi) + \nabla g \times \nabla\phi \tag{25}$$

3.7 Modelling Assumptions

The following simplifying assumptions are applied for dynamical system modelling and stability analysis of the FRC plasma centroid position. Assumptions have been deemed applicable per [12] for tokamak plasmas, review of FRCs [3] and per consultation with PSS.

1. FRC plasma mass (m_p) is constant (plasma assumed to be closed system).
2. Rigid-body FRC dynamics (neglecting high-order plasma dynamic modes).
3. FRC separatrix shape (R_{sep}, Z_{sep}) in plasma body frame is time-invariant.
4. FRC O-point position (magnetic axis) in plasma body frame is time-invariant.
5. Plasma current density ($\vec{J}_p$) is time varying.
6. Purely toroidal plasma current density, no poloidal current ($\vec{J}_p = j_\phi \hat{e}_\phi$).
7. Purely poloidal magnetic field, no toroidal magnetic field ($\vec{B}_p = \vec{B}_\theta,\ \vec{B}_\phi = 0$).
8. Vacuum field (B_v) from copper-EM coils (not flux conserving) is time-invariant
9. Ions carry the plasma mass, electrons carry plasma current (per MHD Figure 7)
10. Flux-conserving currents induced in superconducting coils (axial field coils) are a function of plasma axial position only (radial position negligible effect).

3.8 Modelling Separatrix Geometry

Two separatrix shapes (elliptical and racetrack) are considered for prolate FRC plasmas (Elongation > 1), as shown in Figure 11. The assumption that the separatrix is time invariant per Section 3.7 applies only for FRCs exhibiting “macro-equilibrium” (plasma instabilities do not manifest, plasma pressure in-balance with EM forces, stable shape).

From experimental observations, prolate FRCs exhibit a separatrix shape closer resembling racetrack than elliptical.

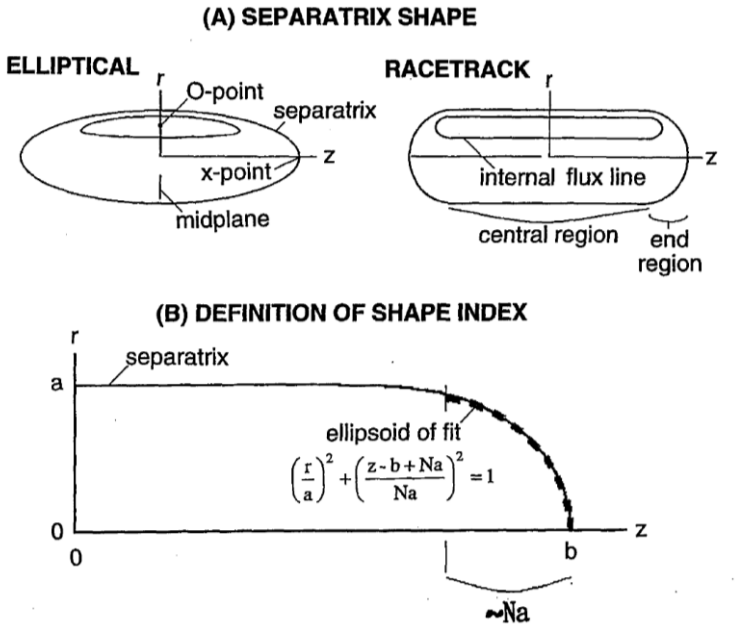

Figure 11. Characteristics of FRC Equilibria: Elliptical and Racetrack Separatrix Shapes [13]

3.8.1 Standardised Separatrix Shape

A Standardised Separatrix Shape is defined in Equation (26) providing an adequate analytical expression and least-square fit to a 'racetrack' separatrix [13], and is compared in Figure 12. Thus, it has been selected for stability and dynamical system analysis.

$$\left(\frac{r^B}{R_{sep}}\right)^2+\left(\frac{z^B}{0.5\cdot Z_{sep}}\right)^{2m}=1 \tag{26}$$

$$m \cong 1.1\frac{E}{N_{sep}}-0.1 \tag{27}$$

Where E is FRC elongation, (r^B, z^B) are radial and axial positions in plasma body frame per Section 3.1, (R_{sep}, Z_{sep}) are separatrix radius and length, exponent 'm' characterises separatrix shape in the end-regions, and N_{sep} is separatrix shape index. N_{sep} = 1 (for ellipsoidal end-region, FRC ends are hemispheres of radius R_{sep}) and N_{sep} = E (separatrix is pure ellipse).

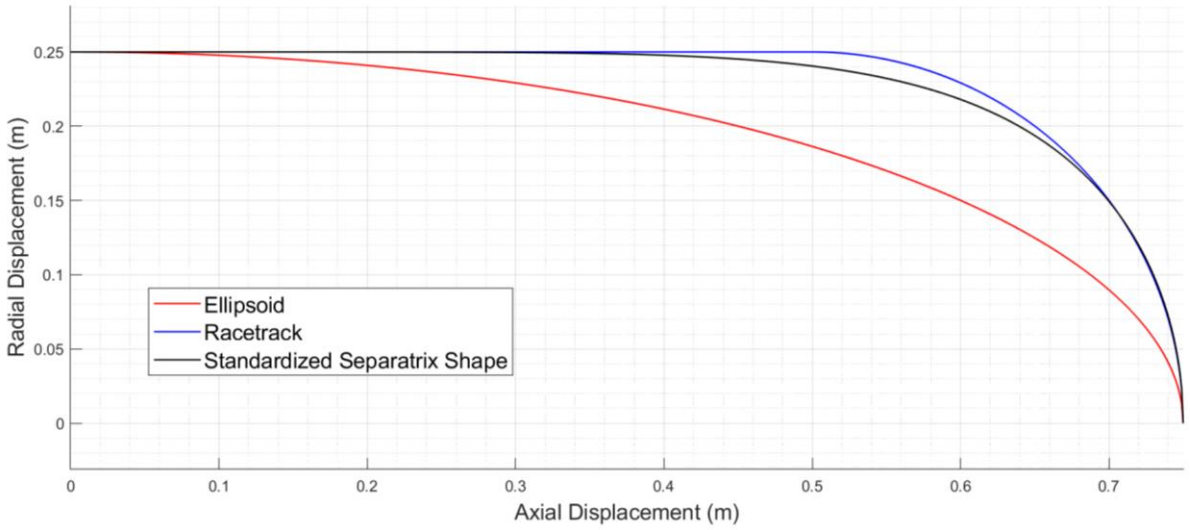

Figure 12. Separatrix Shape Comparison

3.8.2 Modelling FRC Plasma Volume

The volume of a FRC plasma with separatrix shape defined by Equation (26) and (27), is derived as follows (i.e. volume integral for a surface of revolution):

$$V_p = 2\int_0^{0.5\cdot Z_{sep}} \int_0^{2\pi} \int r^B(z^B)\,\mathrm{d}r^B\,\mathrm{d}\phi\,\mathrm{d}z^B$$

$$= 2\int_0^{0.5\cdot Z_{sep}} \int_0^{2\pi} \frac{1}{2} r^B(z^B)^2\,\mathrm{d}\phi\,\mathrm{d}z^B$$

Rearranging Equation (26) for $r^B(z^B)$ and substituting:

$$= \int_0^{0.5\cdot Z_{sep}} \int_0^{2\pi} R_{sep}^2 \left[1 - \left(\frac{z^B}{0.5\cdot Z_{sep}}\right)^{2m}\right] \mathrm{d}\phi\,\mathrm{d}z^B$$

$$= \int_0^{0.5\cdot Z_{sep}} 2\pi\cdot R_{sep}^2 \left[1 - \left(\frac{z^B}{0.5\cdot Z}\right)^{2m}\right] \mathrm{d}z^B$$

$$\therefore V_p = \frac{2\pi\cdot R_{sep}^2\cdot Z_{sep}\cdot m}{(2m+1)} \tag{28}$$

The FRC plasma volume is approximated as follows using Equations (27) and (28), $N_{sep} = 1$ (race-track configuration), and separatrix dimensions specified per Table 5:

$$m = 1.1\left(\frac{3}{1}\right) - 0.1 = 3.2$$

$$V_p = \frac{2\pi \cdot 0.25^2 \cdot 1.5 \cdot 3.2}{(2(3.2)+1)} \cong 0.254724\ \text{m}^3 \tag{29}$$

3.9 Modelling Plasma Current Density

The FRC plasma is assumed to exhibit purely toroidal electric current ($\vec{J}_\theta = \vec{0}$, zero poloidal current) resulting in a purely poloidal magnetic field/flux ($B_\phi = 0$, zero toroidal magnetic field) per assumptions in Section 3.7 and as shown in Figure 1 and Figure 4. Thus, the toroidal flux defined in Equation (16) becomes:

$$B_\phi = 0 \implies g = 0 \tag{30}$$

FRC plasma toroidal current density derived in Equation (22), reduces as assumed to:

$$g = 0 \implies \vec{J}_\theta = \vec{0} \tag{31}$$

FRC total magnetic field derived in Equation (18), reduces to a purely poloidal field:

$$g = 0 \implies \vec{B} = \vec{B}_\theta = \nabla\psi \times \nabla\phi \tag{32}$$

Given the equilibrium conditions derived in Equation (6) for a FRC plasma and assumptions in Equations (30), (31) and (32), FRC plasma pressure is derived per [14] to be:

$$p(\psi) = p_{\max}\left(\frac{\psi_i - \psi}{\psi_i - \psi_a}\right)^{1+\delta} \tag{33}$$

Where $p_{\max}$ is plasma pressure at the magnetic axis (O-point), ψ_i is poloidal flux at the separatrix (plasma-vacuum interface), ψ_a is poloidal flux at the magnetic axis (O-point), δ is shape constant. Noting, FRC exhibits zero plasma pressure at the separatrix, $p(\psi_i) = 0$, and maximum pressure at the magnetic axis/O-point, $p(\psi_a) = p_{\max}$.

The FRC plasma pressure defined in Equation (33) can be reduced to Equation (34), given FRC separatrix shape and O-point are assumed time invariant per Section 3.7, thus relative distances between plasma-vacuum interface and magnetic axis are assumed constant:

$$p(\psi) = p_{\max}\left(\frac{\psi}{\psi_{\max}}\right)^{1+\delta} \tag{34}$$

Note: recalling plasma pressure to be proportional to magnetic field quadratically ($p \sim B^2/2\mu_0$), however, proportional to magnetic flux ψ linearly as shown in Equation (34).

FRC plasma current density is defined in terms of plasma pressure p as follows [15]:

$$j_p(r^B) = r^B \frac{\partial p}{\partial \psi} \tag{35}$$

FRC plasma current density is then derived using Equations (34) and (35) as follows:

$$j_p(r^B) = r^B(1+\delta)p_{\max}\frac{\psi^\delta}{\psi_{\max}^{1+\delta}} \in \mathbb{R}^1 \tag{36}$$

This derivation for FRC plasma current is Solov'ev's Rigid-Rotor Model (RRM), where plasma current density is linear with respect to radial position in plasma body frame r^B. Given the FRC is assumed to be in "macro-equilibrium" (plasma instabilities do not manifest, plasma pressure in-balance with EM forces, stable shape) poloidal flux and plasma current are assumed time-invariant, hence, plasma current could be reduced to the expression $j_p = a_j r^B$.

Given FRC plasma current density is purely toroidal, the vector form is:

$$\vec{j}_p = j_p \hat{e}_\phi \tag{37}$$

An alternate form of Solov'ev's RRM for plasma current density (derived in Equation (36)) is given in [16] as follows, and plotted in Figure 13 for various FRC Elongations:

$$j_p(r^B) = r^B \frac{B_{\max}}{\mu_0 R_{sep}^2}\left(4 + \frac{1}{E^2}\right) \in \mathbb{R}^1 \tag{38}$$

Where $B_{\max}$ is maximum field strength at the separatrix along the FRC midplane and R_{sep}, E are separatrix shape parameters per Table 5.

Thus, FRC plasma current $\vec{J}_p$ for a toroidal differential element ($dA = \mathrm{d}r^B \mathrm{d}z^B$) is as follows, where current density j_p can be per Equation (36) or (38):

$$\vec{J}_p(r^B) = j_p(\mathrm{d}r^B \mathrm{d}z^B)\hat{e}_\phi \in \mathbb{R}^{3\times 1} \tag{39}$$

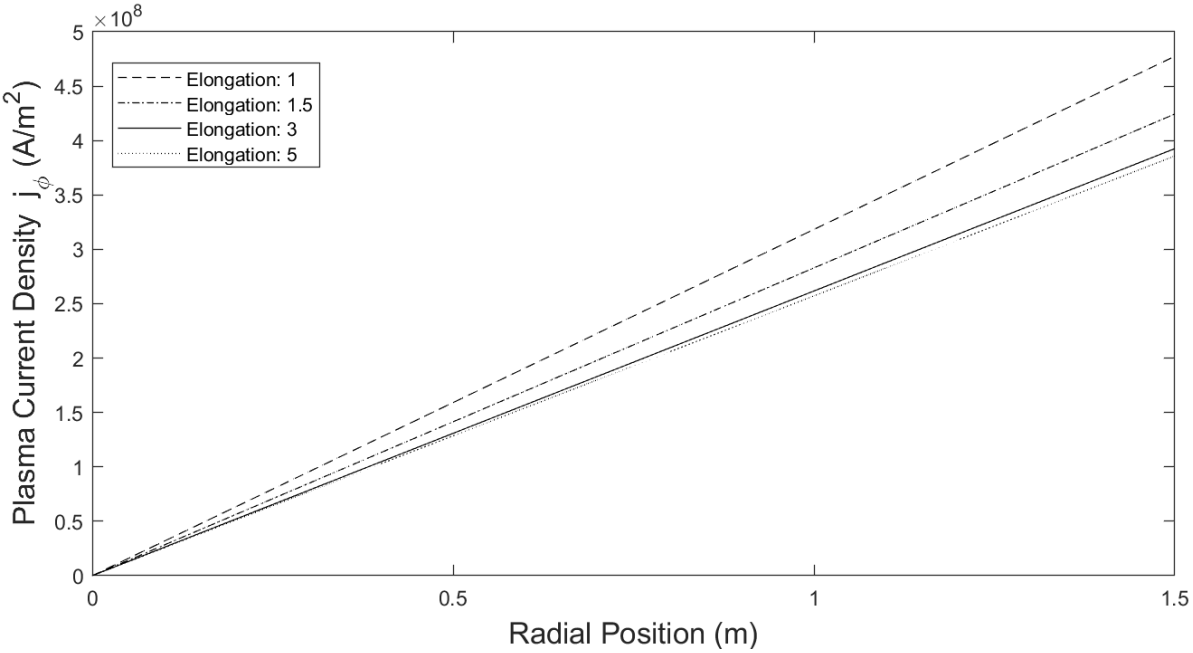

Figure 13. FRC Plasma Current Density, Solov'ev Rigid Rotor Model (RRM)

3.10 Discretisation of Plasma Electric Circuits

Given electrons in the FRC plasma are assumed to carry all the electric current and this current is assumed purely toroidal per Section 3.7, two circuit discretisations are considered:

a) Plasma Current Carrying Coils: plasma is modelled as a set of current carrying coils running toroidally per Figure 14.a, where plasma coil "j" has radius $r^B_{PC_j}$, axial position $z^B_{PC_j}$ (in plasma body frame), current J_{PC_j} and cross-sectional area $dA = \Delta r_p \Delta z_p$. This is used to model *electrical interactions* between FRC plasma coils and actuator coil circuits (see Section 1.2.2.1.b).

b) Plasma Volume Elements: plasma is modelled as differential volume elements as shown in Figure 14.b with volume $dV = r^B \mathrm{d}r^B \mathrm{d}\phi \mathrm{d}z^B$, centroid position (r^B, ϕ, z^B) and current $\vec{J}_p$ acting toroidally at the element centroid. This is used to simulate EM forces acting on plasma elements, and hence total body.

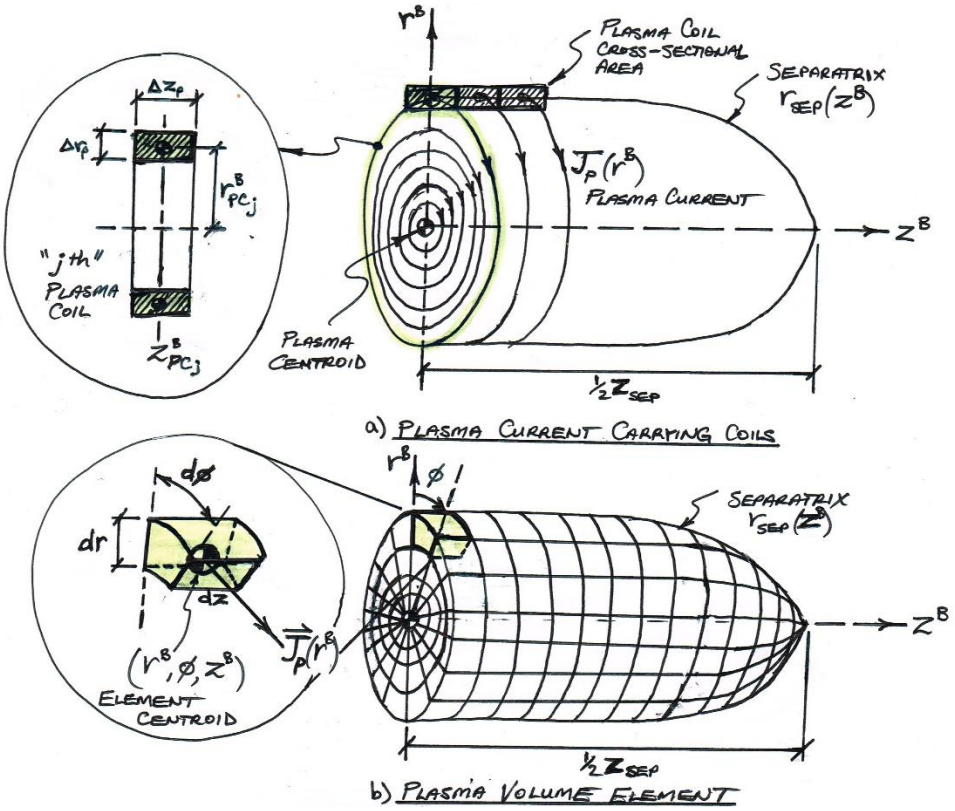

Figure 14. FRC Plasma Discretisation: a) Current Carrying Circuits, b) Volume Elements

3.11 Modelling Mutual Inductance Between Coils

The mutual inductance between two coaxial coils of radius and z-position (r_1, z_1) and (r_2, z_2), with constant-current are given by assuming Maxwell Coils per [17] as follows:

Elliptic Modulus:

$$k = 2\sqrt{\frac{r_1 r_2}{(z_2 - z_1)^2 + (r_2 + r_1)^2}} \qquad \text{where: } k^2 \in (0,1) \tag{40}$$

Complete Elliptic Integral of 1st kind:

$$K_{elliptic} = \int_0^{\frac{\pi}{2}} (1 - k^2 \sin^2\theta)^{-\frac{1}{2}}\, d\theta \tag{41}$$

$$= \int_0^1 \frac{1}{(1 - t^2)(1 - k^2 t^2)}\, dt$$

Complete Elliptic Integral of 2nd kind:

$$E_{elliptic} = \int_0^{\frac{\pi}{2}} (1 - k^2 \sin^2\theta)^{\frac{1}{2}}\, d\theta \tag{42}$$

$$= \int_0^1 \frac{\sqrt{1 - k^2 t^2}}{\sqrt{1 - t^2}}\, dt$$

Thus, the mutual inductance between coils 1 and 2 is given by the elliptic integral:

$$M_{1,2} = \frac{2\mu_0\sqrt{r_1 r_2}}{k}\left[\left(1 - \frac{1}{2}k^2\right)K_{elliptic} + E_{elliptic}\right] \in \mathbb{R}^1 \tag{43}$$

3.11.1 Modelling Mutual Inductance Between Coil Actuators and FRC Plasma

Given axial field coils in Figure 3 are superconducting (overview in Section 1.2.2.1.b), flux-conserving currents (induced by plasma flux) are assumed to be a function of only plasma

axial-position (per Section 3.7), superconducting coils are coaxial, have constant current and rectangular cross-section, and plasma discretisation per Section 3.10.a); therefore, plasma coils and actuator coils can be modelled as Maxwell Coils (similar to [18]) and Equation (43) applies.

Given:

r_{C_i} radius of axial field coil 'i' per Figure 6.

$z^I_{C_\mathrm{i}}$ axial position of axial field coil 'i' in inertial frame per Figure 6.

r_{PC_j} radius of plasma coil "j" per Figure 14.a.

$z^B_{PC_j}$ axial position of plasma coil "j" in plasma body frame per Figure 14.a.

z^I_{CEN} axial position of FRC plasma centroid in inertial frame per Figure 6.

N_C the number of superconducting coils.

N_{PC} the number of plasma coils (plasma body discretised into N_p coils).

For Equations (40) to (43), Let:

Coil 1: $(r_1, z_1) \coloneqq \left(r_{C_\mathrm{i}},\ z^I_{C_\mathrm{i}}\right)$ superconducting coil "i"

Coil 2: $(r_2, z_2) \coloneqq \left(r_{PC_j},\ z^I_{CEN} + z^B_{PC_j}\right)$ plasma coil "j"

The mutual inductance between axial field coil "i" and plasma coil "j" is thus given by:

$$M_{C_i,PC_j} = \frac{2\mu_0\sqrt{r_{C_i} r_{PC_j}}}{k}\left[\left(1 - \frac{1}{2}k^2\right)K_{elliptic} + E_{elliptic}\right] \in \mathbb{R}^1 \tag{44}$$

$$\text{where: } i \in \{1, \dots, N_C\},\ \ j \in \{1, \dots, N_{PC}\}$$

The mutual inductance between all superconducting coils and plasma coils given by Equation (44) is expressed in compact notation as follows (i.e. $\forall i, j$):

$$\vec{M}_{C,PC} \in \mathbb{R}^{N_C \times N_{PC}} \tag{45}$$

N.B. mutual inductance in Equation (44) is deemed appropriate for numerical simulation and analysis, however, it is not closed (analytical) form due to elliptic integrals and thus inadequate for stability analysis. Mutual inductance can be approximated through methods outlined in [19] to convert to analytical form, this is captured in Chapter 7.2 as future work.

3.11.2 Modelling Mutual Inductance of Coil Actuators

The mutual inductance between superconducting coils "i" and "j" is given by Equations (40) to (43). Noting, mutual inductance exhibits the following symmetry:

$$\mathrm{M}_{C_i,C_j} = \mathrm{M}_{C_j,C_i} \quad \forall i, j \in \{1, \dots, N_C\} \quad \Longrightarrow \quad \vec{M}_{C,C} = \vec{M}_{C,C}^{T} \tag{46}$$

Thus, the mutual inductance matrix of superconducting coils is square symmetric:

$$\vec{M}_{C,C} = \left\{ \vec{X} \in \mathbb{R}^{N_C \times N_C} \mid \vec{X} = \vec{X}^{T} \right\} \tag{47}$$

Where elements:
$i = j$ (diagonal entries) is the self-inductance of superconducting coil "i"

$i \neq j$ is the mutual inductance between superconducting coils "i" and "j"

3.11.3 Modelling Self-Inductance of Coil Actuators

The self-inductance of superconducting axial field coils in Figure 3 is found by setting coils 1 and 2 to be equal in Equations (40) to (43). For example, Let: $(r_1, z_1) = (r_2, z_2) = \left(r_{C_\mathrm{i}}, z_{C_\mathrm{i}}^{I}\right)$ for superconducting coil "i".

3.12 Modelling Magnetic Flux through Superconducting Coils due to FRC Plasma

The magnetic flux through each superconducting coil due to electric currents in the FRC plasma is given in compact notation as:

$$\vec{\Phi}_{C,PC} = \vec{M}_{C,PC}\,\vec{J}_{PC} \tag{48}$$

Where:
$\vec{\Phi}_{C,PC} \in \mathbb{R}^{N_C \times 1}$ magnetic flux (Wb) through each superconducting coil due to plasma.

$\vec{M}_{C,PC} \in \mathbb{R}^{N_C \times N_{PC}}$ is mutual inductance matrix (H) between all superconducting coils and plasma coils per Equation (45).

$\vec{J}_{PC} \in \mathbb{R}^{N_{PC} \times 1}$ is the electric current (A) through each of the N_{PC} plasma coils.

For example, the magnetic flux through superconducting coil "i" due to the entire FRC plasma is given by ith row of Equation (48) with $\vec{M}_{C_i,PC} \in \mathbb{R}^{1 \times N_{PC}}$ given by ith row of Equation (45) as follows:

$$\Phi_{C_i,PC} = \vec{M}_{C_i,PC}\,\vec{J}_{PC} \in \mathbb{R}^1 \qquad i \in \{1, \dots, N_C\} \tag{49}$$

N.B. Biot-Savart law can be employed as an alternative for more complex actuator circuit geometries and magnetic field topologies (non-coaxial coils such as saddle coils). This is captured in Chapter 7 as future work. Magnetic flux formulation is currently deemed adequate for stability analysis of coaxial coils and significantly faster for simulation.

3.13 Modelling Flux-Conserving (FC) Currents through Superconducting Coils

The magnetic flux through superconducting coils is required to be zero due to flux conservation (refer Section 1.2.2.1.b).

The flux conserving electric current in superconducting coils required to counteract plasma flux is derived as follows:

$$\vec{\Phi}_{C,PC} = \vec{M}_{C,C}\,\vec{I}_{FC}$$

$$\vec{I}_{FC} = \vec{M}_{C,C}^{-1}\,\vec{\Phi}_{C,PC} \tag{50}$$

Where:
$\vec{I}_{FC} \in \mathbb{R}^{N_C \times 1}$ is flux-conserving current (A) through each superconducting coil.

$\vec{M}_{C,C} \in \mathbb{R}^{N_C \times N_C}$ is mutual inductance matrix (H) of SC coils, per Section 3.11.2.

$\vec{\Phi}_{C,PC}$ is the magnetic flux (Wb) through SC coils due to plasma, per Equation (63).

Thus, the superconducting coil currents induced due to plasma magnetic flux is given by subtracting FC current per Equation (50) (thus rationale for minus sign):

$$\vec{I}_C = \vec{I}_{\overline{\mathrm{FC}}} - \vec{I}_{FC}$$

$$= \vec{I}_{\overline{\mathrm{FC}}} - \vec{M}_{C,C}^{-1}\,\vec{\Phi}_{C,PC} \tag{51}$$

Where:
$\vec{I}_C \in \mathbb{R}^{N_C \times 1}$ is total electric current (A) through each superconducting coil.

$\vec{I}_{FC} \in \mathbb{R}^{N_C \times 1}$ is flux-conserving current (A) through each superconducting coil.

$\vec{I}_{\overline{\mathrm{FC}}} \in \mathbb{R}^{N_C \times 1}$ is non-FC electric current (A) through each superconducting coil.

$\vec{M}_{C,C} \in \mathbb{R}^{N_C \times N_C}$ is mutual inductance matrix (H) of SC coils, per Section 3.11.2.

$\vec{\Phi}_{C,PC}$ is the magnetic flux (Wb) through SC coils due to plasma, per Equation (63).

N.B. Flux conserving currents are only a function of FRC axial-pos. per Section 3.7.

3.14 Modelling Magnetic Flux through FRC Plasma due to Superconductor Currents

The magnetic flux through the FRC plasma due to superconducting coil currents (flux conserving currents) is given in compact notation as:

$$\vec{\Phi}_{PC,C} = \vec{M}_{PC,C}\,\vec{I}_C \tag{52}$$

Where:
$\vec{\Phi}_{PC,C} \in \mathbb{R}^{N_{PC}\times 1}$ is magnetic flux (Wb) through each plasma coil due to SC coil currents

$\vec{M}_{PC,C} = \vec{M}^{\mathrm{T}}_{C,PC} \in \mathbb{R}^{N_{PC}\times N_C}$ is mutual inductance matrix (H) b/w plasma and SC coils

$\vec{I}_C \in \mathbb{R}^{N_C\times 1}$ is total electric current (A) through each superconducting coil.

N.B. Flux $\vec{\Phi}_{PC,C}$ acts at the centre of plasma coils.

The radial and axial magnetic field through the FRC plasma due to superconducting coil currents is given by:

$$\begin{aligned} \vec{B}_{C_r} &= \vec{\Phi}_{PC,C}\,\vec{S}_r \\ \vec{B}_{C_z} &= \vec{\Phi}_{PC,C}\,\vec{S}_z \end{aligned} \tag{53}$$

Where:
$\vec{B}_{C_r}, \vec{B}_{C_z} \in \mathbb{R}^{N_{PC}\times 1}$ is magnetic field (T) acting on FRC plasma due to SC coil currents.

$\vec{S}_r, \vec{S}_z$ radial and axial spatial derivatives computed by a finite element grid solver [20].

3.15 Modelling Total External Magnetic Field

The total external magnetic field acting on the FRC plasma comprises of two components (summarised in Table 3): a vacuum field component $\vec{B}^{I}_{\mathrm{v}}$ (assumed time-invariant per Section 3.7, due to constant-current copper EM coil, exists if plasma was removed), and

flux-conserving field component $\vec{B}_C^I$ (time-varying per Section 3.7, due to superconducting coils and axial-position of the FRC z_{CEN}^I) per Equation (53), given as follows in inertial frame:

$$\begin{aligned} B_r^I &= B_{\mathrm{v}_r}^I + B_{C_r}^I \\ B_z^I &= B_{\mathrm{v}_z}^I + B_{C_z}^I \\ \vec{B}^I &= \vec{B}_{\mathrm{v}}^I + \vec{B}_C^{\mathrm{I}} = \begin{bmatrix} B_r^I \\ 0 \\ B_z^I \end{bmatrix} \in \mathbb{R}^{3\times 1} \end{aligned} \tag{54}$$

N.B. The radial vacuum field $B_{\mathrm{v}_r}^I$ exhibits sign-reversal about the machine midplane (inertial z-axis) as follows:

$$\begin{aligned} B_{\mathrm{v}_r}^I &< 0 \quad \text{for } z^I > 0 \quad \text{(negative vacuum field, right of PFRC midplane)} \\ B_{\mathrm{v}_r}^I &> 0 \quad \text{for } z^I < 0 \quad \text{(positive vacuum field, left of PFRC midplane)} \end{aligned} \tag{55}$$

Table 3. Dependency of Magnetic Field Components on FRC Perturbations

Magnetic Field Component	Type of FRC Pos. Perturbation	Field Impact
Vacuum Field ($\boldsymbol{B_{\mathrm{v}}^I}$) (EM coils)	Any perturbation (radial or axial)	No Variation
Flux-Conserving Field ($\boldsymbol{B_C^I}$) (SC coils)	No Axial Perturbation	
	Axial Perturbation	Recompute

3.16 Modelling FRC Plasma Centroid Position

Let the state vector for the FRC plasma model be as follows and illustrated in Figure 6:

$$\vec{x} = \begin{bmatrix} \vec{\xi}_{\mathrm{CEN}}^I \\ \dot{\vec{\xi}}_{\mathrm{CEN}}^I \end{bmatrix} = \begin{bmatrix} x_{\mathrm{CEN}}^I \\ y_{\mathrm{CEN}}^I \\ z_{\mathrm{CEN}}^I \\ \dot{x}_{\mathrm{CEN}}^I \\ \dot{y}_{\mathrm{CEN}}^I \\ \dot{z}_{\mathrm{CEN}}^I \end{bmatrix} \in \mathbb{R}^{6\times 1} \tag{56}$$

Where:
$\vec{\xi}_{\mathrm{CEN}}^I = [x_{\mathrm{CEN}}^I \; y_{\mathrm{CEN}}^I \; z_{\mathrm{CEN}}^I]^{\mathrm{T}} \in \mathbb{R}^{3\times 1}$ is the FRC centroid position in inertial frame.

$\dot{\vec{\xi}}^I_{\text{CEN}} = [\dot{x}^I_{\text{CEN}}\ \dot{y}^I_{\text{CEN}}\ \dot{z}^I_{\text{CEN}}]^{\text{T}} \in \mathbb{R}^{3\times 1}$ is the FRC centroid velocity in inertial frame.

The net force acting on the FRC plasma centroid is given as follows, provided that the FRC plasma is "self-consistent" (plasma poloidal magnetic field is balanced with plasma pressure per Equation (6)), assuming a rigid-body plasma per Section 3.7, plasma current given by Equation (39) and external magnetic field given by Equation (54):

$$\vec{F}_{\text{CEN}} = m_p \frac{d\dot{\vec{\xi}}^I_{CEN}}{dt} = \int \vec{J}_p \times \vec{B}^I \ dV_p \tag{57}$$

The differential volume element dV_p in cylindrical coordinates per Equation (66) gives:

$$\vec{F}_{\text{CEN}} = m_p \frac{d\dot{\vec{\xi}}^I_{CEN}}{dt} = \int_{-\frac{1}{2}Z_{sep}}^{\frac{1}{2}Z_{sep}} \int_0^{2\pi} \int_0^{r^B_{sep}(z^B)} \left(\vec{J}_p \times \vec{B}^I\right)\ r^B \mathrm{d}r^B \mathrm{d}\phi \mathrm{d}z^B \tag{58}$$

Given Equation (58) is not a closed-form expression (due to mutual inductances $\vec{M}_{PC,C}$ and $\vec{M}_{C,C}$ in the magnetic field term $\vec{B}^I$) the net Lorentz force is numerically integrated over a discretised volume. The FRC plasma is discretised by differential volume elements outlined in Section 3.10.b) and illustrated in Figure 14.b. The position of a plasma volume element is given in inertial frame as:

$$\vec{\xi}^I_p = \vec{\xi}^I_{CEN} + \vec{\xi}^B_p = \begin{bmatrix} x^I_p \\ y^I_p \\ z^I_p \end{bmatrix} \tag{59}$$

Where $\vec{\xi}^B_p$ is the position of a volume element's centroid, in plasma body frame (this is treated as a model parameter). Let the xy-position (radial position) of a plasma element in inertial frame and its unit vector be denoted as:

$$\vec{\xi}_{p_{xy}}^{I} = \begin{bmatrix} x_p^I \\ y_p^I \end{bmatrix} \in \mathbb{R}^{2\times 1} \qquad \hat{\xi}_{p_{xy}}^{I} = \frac{\vec{\xi}_{p_{xy}}^{I}}{\left\| \vec{\xi}_{p_{xy}}^{I} \right\|} \tag{60}$$

The direction vector $\hat{\xi}_{p_{xy}}^{I}$ is used to apply the radial component of external magnetic field B_r^I to compute the Lorentz force on a plasma differential volume element as follows:

$$\vec{B}_{xy}^{\mathrm{I}} = B_r^I \hat{\xi}_{p_{xy}}^{I} \tag{61}$$

The net magnetic field acting on a plasma differential volume element "i" is thus:

$$\vec{B}_i = \begin{bmatrix} \vec{B}_{xy}^{I} \\ \vec{B}_z^I \end{bmatrix} \in \mathbb{R}^{3\times 1} \tag{62}$$

3.17 Modelling Plasma Inertial Mass

Given time invariant separatrix shape and rigid-body plasma dynamics per simplifying assumptions in Section 3.7, the FRC plasma mass (mass of all particles) is expressed as:

$$m_p = \int \frac{n_p M_p}{N_A} dV_p \cong \frac{n_p M_p}{N_A} V_p \tag{63}$$

Given chemical properties specified per Table 6, FRC plasma volume (V_p) per Equation (29) assuming a racetrack separatrix shape (illustrated in Figure 11), FRC plasma mass is thus approximated as:

$$m_p \cong \frac{4 \times 10^{20} \left|\frac{\text{ions}}{\text{m}^3}\right| \cdot 2.5 \times 10^{-3} \left|\frac{\text{kg}}{\text{mol}}\right|}{6.022 \times 10^{23} \left|\frac{\text{ions}}{\text{mol}}\right|} \cdot 0.25472 \, |\text{m}^3| \cong 4.2299 \times 10^{-7} \text{ kg} \tag{64}$$

N.B. the fuel ratio D:He3 remains an open area of study, with 1:3 being considered the best candidate thus far [11] and impacts plasma molar mass (M_p) and number density (n_p).

Chapter 4. Dynamical System Model Overview

4.1 Overview of Model Equations

An overview of the dynamical system model derived in this Thesis for the FRC plasma centroid position is provided in Table 4 with assumptions listed in Section 3.7. References to derivations are included, along with identification of state variables and parameters.

Table 4. Overview of Dynamical System Model

Dynamics Description	Var.	Param.	Dynamics Equation	Ref.
Plasma Separatrix Shape (r^B, z^B) Separatrix Shape Exponent (m)	r^B z^B	R_{sep} Z_{sep} N_{sep} E	$\left(\frac{r^B}{R_{sep}}\right)^2 + \left(\frac{z^B}{Z_{sep}}\right)^{2m} = 1$ $m \cong 1.1\frac{E}{N_{sep}} - 0.1$	(26) (27)
Plasma Volume (V_p)	-	R_{sep} Z_{sep}	$V_p = \frac{2\pi \cdot R_{sep}^2 \cdot Z_{sep} \cdot m}{(2m+1)}$	(28)
Plasma Mass (m_p)	-	M_p n_p N_A	$m_p = \int \frac{n_p M_p}{N_A} dV_p \cong \frac{n_p M_p}{N_A} V_p$	(63)
Plasma Pressure (P)	-	δ ψ $\psi_{\max}$ $P_{\max}$	$P(\psi) = P_{\max}\left(\frac{\psi}{\psi_{\max}}\right)^{1+\delta}$	(34)
Plasma Current Density $(\vec{J}_p)$	r^B	δ ψ $\psi_{\max}$ $P_{\max}$	$j_p = r^B(1+\delta)P_{\max}\frac{\psi^\delta}{\psi_{\max}^{1+\delta}}$ $\vec{J}_p = j_p \hat{e}_\phi$	(36) (37)
Plasma Current $(\vec{J}_p)$	r^B	-	$\vec{J}_p = j_p(\mathrm{d}r^B \mathrm{d}z^B)\hat{e}_\phi$	(39)
Mutual inductance between Coaxial Coils 1 and 2 $(M_{1,2})$	-	-	$M_{1,2} = \frac{2\mu_0\sqrt{r_1 r_2}}{k}\left[\left(1-\frac{1}{2}k^2\right)K_{elliptic} + E_{elliptic}\right]$	(43)

Table 4. Overview of Dynamical System Model, Continued

Dynamics Description	Var.	Param.	Dynamics Equation	Ref.
Elliptic Modulus (k) Complete Elliptic Integral of 1st & 2nd kind ($K_{elliptic}, E_{elliptic}$)	-	-	$k = 2\sqrt{\frac{r_1 r_2}{(z_2 - z_1)^2 + (r_2 + r_1)^2}}$ $K_{elliptic} = \int_0^1 \frac{1}{(1-t^2)(1-k^2t^2)}\, dt$ $E_{elliptic} = \int_0^1 \frac{\sqrt{1-k^2t^2}}{\sqrt{1-t^2}} dt$	(40) (41) (42)
Mutual Inductance b/w Superconducting Coils and FRC Plasma ($\vec{M}_{C,PC}$)	z^I_{CEN}	μ_0 r_{C_i} z_{C_i} r_{PC_j} z_{PC_i}	$M_{C_i,PC_j} = \frac{2\mu_0\sqrt{r_{C_i} r_{PC_j}}}{k}\left[\left(1 - \frac{1}{2}k^2\right) K_{elliptic} + E_{elliptic}\right]$ where: $i \in \{1, \ldots, N_C\},\ j \in \{1, \ldots, N_{PC}\}$ $\vec{M}_{C,PC} \in \mathbb{R}^{N_C \times N_{PC}}$	(44) (45)
Mutual Inductance of Superconducting coils ($\vec{M}_{C,C}$)	-	-	$\vec{M}_{C,C} = \left\{\vec{X} \in \mathbb{R}^{N_C \times N_C} \mid \vec{X} = \vec{X}^T\right\}$	3.11.2 (47)
FRC Plasma Magnetic Flux through Superconducting Coil ($\vec{\Phi}_{C,PC}$)	z^I_{CEN}	-	$\vec{\Phi}_{C,PC} = \vec{M}_{C,PC}\, \vec{J}_{PC}$	(48)
Superconducting Flux-Conserving Current ($\vec{I}_{FC}$)	z^I_{CEN}	-	$\vec{I}_{FC} = \vec{M}^{-1}_{C,C}\, \vec{\Phi}_{C,PC}$	(50)
Superconducting Total Coil Current ($\vec{I}_{\mathrm{C}}$)	z^I_{CEN}	-	$\vec{I}_{\mathrm{C}} = \vec{I}_{\overline{\mathrm{FC}}} - \vec{I}_{FC}$	(51)
Superconducting Coil Magnetic Flux through FRC Plasma ($\vec{\Phi}_{PC,C}$)	z^I_{CEN}	-	$\vec{\Phi}_{PC,C} = \vec{M}^{\mathrm{T}}_{C,PC}\, \vec{I}_C$	(52)
Superconducting Coil Magnetic Field through FRC Plasma ($\vec{B}_{C_r}, \vec{B}_{C_z}$)	z^I_{CEN}	$\vec{S}_r$ $\vec{S}_z$	$\vec{B}_{C_r} = \vec{\Phi}_{PC,C}\, \vec{S}_r$ $\vec{B}_{C_z} = \vec{\Phi}_{PC,C}\, \vec{S}_z$	(53)
Total External Magnetic Field in Inertial Frame ($\vec{B}^I$)	z^I_{CEN}	-	$B^I_r = B_{\mathrm{v}_r} + B_{C_r}$ $B^I_z = B_{\mathrm{v}_z} + B_{C_z}$ $\vec{B}^I = [B^I_r, 0, B^I_z]^{\mathrm{T}}$	(54)

Table 4. Overview of Dynamical System Model, Continued

Dynamics Description	Var.	Param.	Dynamics Equation	Ref.
Resultant Force on FRC Plasma Centroid ($\vec{F}_{CEN}$)	x^I_{CEN} y^I_{CEN} z^I_{CEN}	m_p R_{sep} Z_{sep}	$\vec{F}_{CEN} = m_p \frac{d\dot{\vec{\xi}}^I_{CEN}}{dt}$ $= \int_{-\frac{1}{2}Z_{sep}}^{\frac{1}{2}Z_{sep}} \int_0^{2\pi} \int_0^{r^B_{sep}(z^B)} (\vec{J}_p \times \vec{B}^I)\, r^B \mathrm{d}r^B \mathrm{d}\phi \mathrm{d}z^B$	(58)
State Vector ($\vec{x}$)	-	-	$\vec{x} = \begin{bmatrix} \vec{\xi}^I_{\text{CEN}} \\ \dot{\vec{\xi}}^I_{\text{CEN}} \end{bmatrix} \in \mathbb{R}^{6\times 1}$ $= [x^I_{\text{CEN}}, y^I_{\text{CEN}}, z^I_{\text{CEN}}, \dot{x}^I_{\text{CEN}}, \dot{y}^I_{\text{CEN}}, \dot{z}^I_{\text{CEN}}]^{\mathrm{T}}$	(56)

Plasma parameters identified in this model are considered time-invariant per Section 3.7, whereby the FRC plasma is assumed to maintain equilibrium conditions per Equation (6). **Important Note:** notice magnetic field/flux terms $\vec{B}$, $\vec{\Phi}$ and mutual inductance terms $\vec{M}_{C,PC}$ are dependent only on plasma axial position (z^I_{CEN}) for the given coaxial coil configuration.

4.2 Dynamical System Model Parameters

System parameters are provided in Table 5 and Table 6, and are specified by PSS for a PFRC reactor configuration scaled for 1-10 MW power output.

Table 5. Direct Fusion Drive (DFD) and FRC Parameters

Variable / Parameter	Symbol	Value
Separatrix Radius	R_{sep}	0.25m
Separatrix Length	Z_{sep}	1.5m
Elongation ($z_{\text{sep}}/2r_{\text{sep}}$)	E	~3 (prolate)
O-point Radial Position	r_o	0.091cm
X-point Axial Position	z_X	0.75m
Number of Axial Coils	N	12
Magnetic Field Strength, Axial	B_{v_z}	5-7T
Magnetic Field Strength, Nozzle	B_N	20T
Separatrix Shape Index (end-regions)	N_{sep}	1 (ellipsoidal)

Table 6. FRC Plasma Chemical Properties

Variable / Parameter	Symbol	Value
Ion Species	-	D-^{3}He
Fuel Ratio (D:^{3}He)	-	1:3
Plasma Number Density	n_p	4×10^{20} ions/m^3
Plasma Molar Mass (fuel ratio 1:1)	M_p	2.5×10^{-3} kg/mol
Avogadro number	N_A	6.022×10^{23} mol^{-1}

Chapter 5. Numerical Simulation

5.1 Overview of Solver Algorithm

The FRC plasma model in Table 4 to Table 6 is numerically simulated as follows:

1. Initialise time-invariant model parameters identified in Table 4 to Table 6:

    1.1. Vacuum field (B_v), plasma poloidal flux and plasma separatrix shape (ψ, ψ_{max}, P_{max}) are initialised by a *Grad-Shafranov Equilibrium* solver supplied by PSS, which produces a "self-consistent" FRC (plasma current and poloidal field balance out plasma pressure gradient, Equation (6)).

    Note on Plasma Separatrix Shape: From Table 4, the separatrix shape (Equations (26), (27)) is the only expression not implemented in the numerical solver, and intended for analytical control system design/stability analysis (future work). Separatrix shape is instead initialised by PSS' Grad-Shafranov equilibrium, seen in Figure 17, and may be parametrised or curve-fit by Equations (26), (27), recalling it is assumed time-invariant.

    1.2. Calculate mutual inductance between superconducting coils ($\overrightarrow{\boldsymbol{M}}_{\boldsymbol{C,C}}$), Section 3.11.2.

2. Initialise state vector ($\vec{\boldsymbol{x}}$), Equation (56). Run ODE113 solver on steps 3 to 7:

3. Calculate flux-conserving currents (assumed dependent on FRC centroid axial position only), with discretised plasma coils per Figure 14.a:

    3.1. Calculate mutual inductance b/w plasma and superconducting coils ($\overrightarrow{\boldsymbol{M}}_{\boldsymbol{C,PC}}$), Eqn. (45)

    3.2. Calculate flux through superconducting coils due to plasma ($\overrightarrow{\boldsymbol{\Phi}}_{\boldsymbol{C,PC}}$), Eqn. (48)

    3.3. Calculate flux-conserving and superconducting currents ($\vec{\boldsymbol{I}}_{\boldsymbol{FC}}, \vec{\boldsymbol{I}}_{\boldsymbol{C}}$), Equations (50), (51)

4. Calculate magnetic flux through plasma due to superconducting coil ($\vec{\boldsymbol{\Phi}}_{\boldsymbol{PC,C}}$), Equation (52)

5. Calculate magnetic field through plasma due to superconducting coils ($\vec{\boldsymbol{B}}_{\boldsymbol{C_r}}$), Equation (53).

6. Calculate magnetic field through plasma due to vacuum and SC coils ($\vec{\boldsymbol{B}}^{\boldsymbol{I}}$), Equation (54).

7. Calculate resultant force on plasma centroid ($\vec{\boldsymbol{F}}_{\boldsymbol{CEN}}$), Equation (58), with discretised plasma volume per Figure 14.b.

5.2 Vacuum Magnetic Field

The vacuum magnetic field, denoted $\vec{B}_{\mathrm{v}}$ in Equation (54), is simulated by constant-current copper coil actuators, and has axial and radial field components per Figure 15 and Figure 16. These fields are simulated as time-invariant per Section 3.7. Fields are shown here for the "top-right quadrant" of the DFD setup shown in Figure 3.

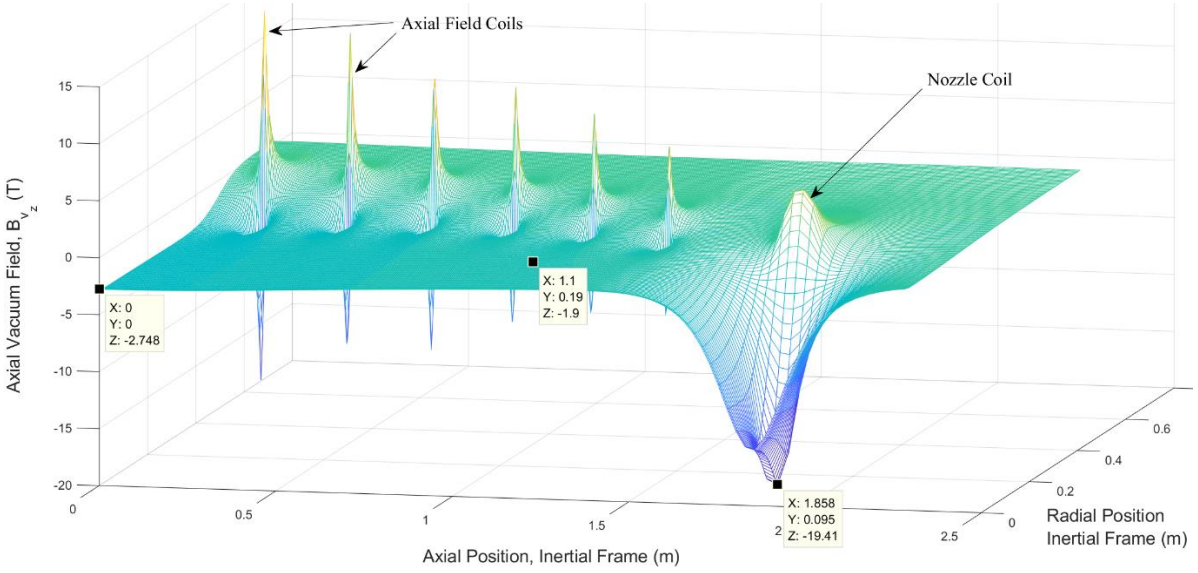

Figure 15. Axial Magnetic Field (Time-Invariant Vacuum Field)

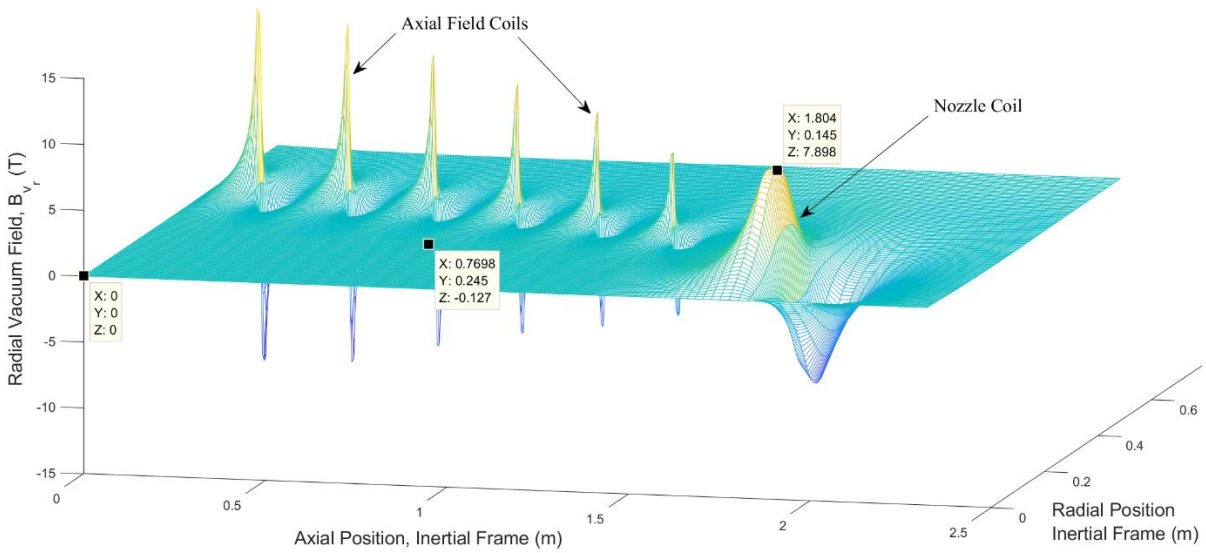

Figure 16. Radial Magnetic Field (Time-Invariant Vacuum Field)

As shown above, constant-current axial field coils and a nozzle coils produce a deep "magnetic well" about the machine origin (r=0, z=0), also nozzle coils are verified in Figure 15 to produce $B_N \cong 20\text{T}$ per Table 5.

Performing a consistency check, the force density acting on a plasma element given the vacuum field $\vec{B}_{\text{v}}$ is expanded per Equation (57) as follows:

$$\vec{f}_p^{\text{I}} = \vec{J}_p \times \vec{B}_{\text{v}}^I = \begin{bmatrix} J_y B_{\text{v}_z}^I \\ -J_x B_{\text{v}_z}^I \\ J_x B_{\text{v}_y}^I - J_y B_{\text{v}_x}^I \end{bmatrix} \tag{65}$$

Evidently, the axial component of the vacuum field ($B_{\text{v}_z}^I$) only dictates the radial motion of a plasma element, and hence the entire rigid-body FRC plasma. The radial components ($B_{\text{v}_x}^I$, $B_{\text{v}_y}^I$) dictate axial motion of the FRC plasma.

On further inspection of Figure 15, the vacuum field has *negative* axial component throughout the entire confinement region and about the origin ($B_{\text{v}_z}^I < 0$). From Equation (65), sign(J_x) and sign(J_y) are always such that toroidal FRC plasma current is a positive-rotation

about the inertial z-axis (by right hand rule). Thus, net force can only be *radially restoring* if $B^I_{\mathrm{v}_z} < 0$. Alternatively, for a vacuum field with *positive* axial component, or a FRC with current in the opposite direction (negative toroidal direction), net force would be *radially destabilising*.

Time-invariant system parameters, such as actuator coil configuration, vacuum magnetic field, FRC plasma separatrix shape, are initialised as shown in Figure 17.

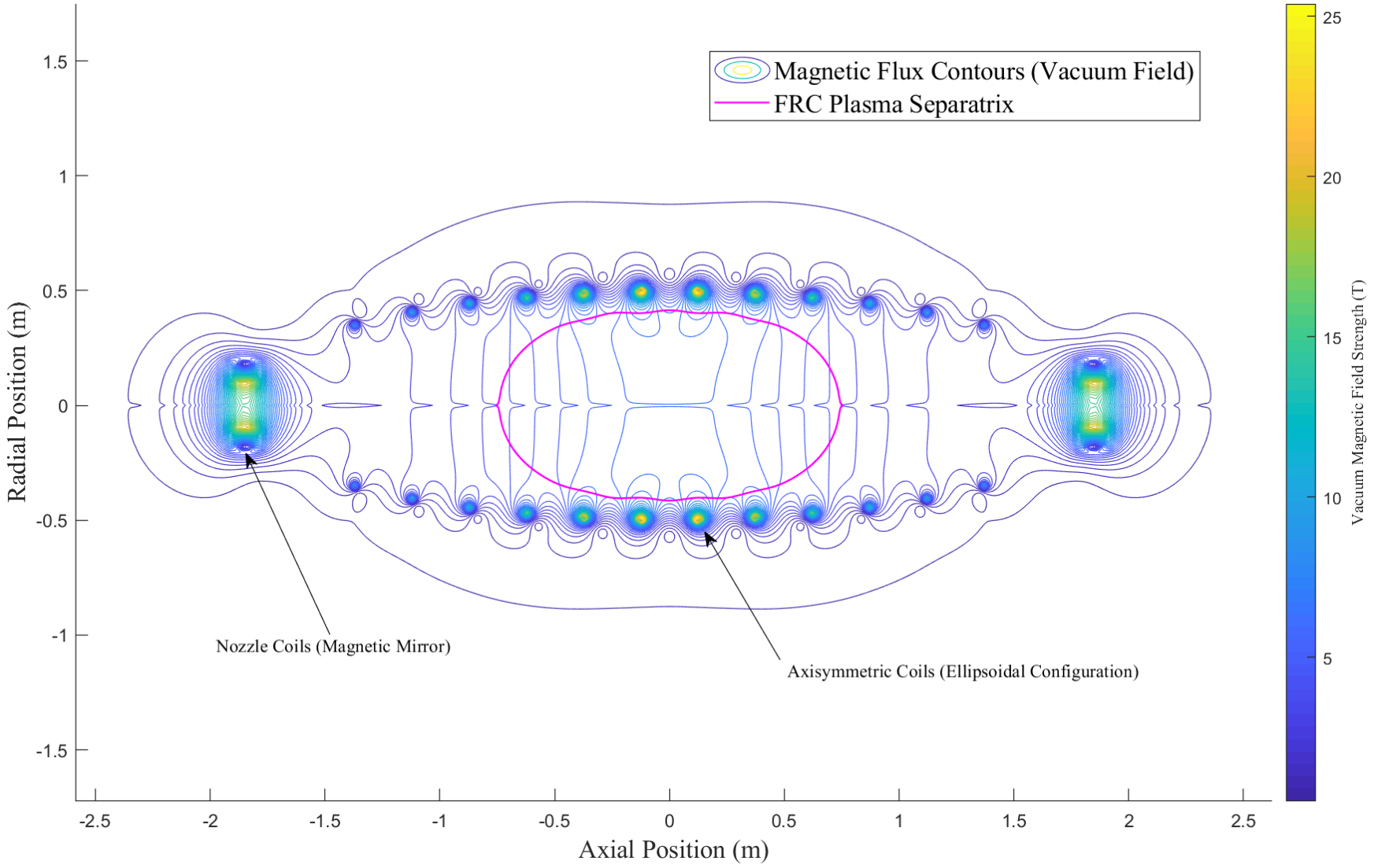

Figure 17. Prolate (E > 1) FRC Plasma in Vacuum Magnetic Field

5.3 Result 1: Plasma Response to Radial Perturbation (Constant Current EM Coils)

The FRC centroid position response to *radial perturbations* (0.5cm, 1cm, 3cm, applied to initial position) is demonstrated in Figure 18. FRC radial position oscillates about the origin at constant frequency without damping, these closed trajectories potentially indicate the system exhibits limit cycling about ICs (unknown stability, neither decaying nor growing). The FRC position and net force in cartesian frame is given in Figure 19, where FRC axial position (subplot: *"Plasma Z-Pos"*) is shown to exhibit random walk on the order of 1×10^{-17}m, attributed to integration of forces on order of 1×10^{-11} N (subplot: *"Resultant Z-Force"*) and likely due to numerical precision errors (consistent for double-precision floating-point) and/or plasma discretisation.

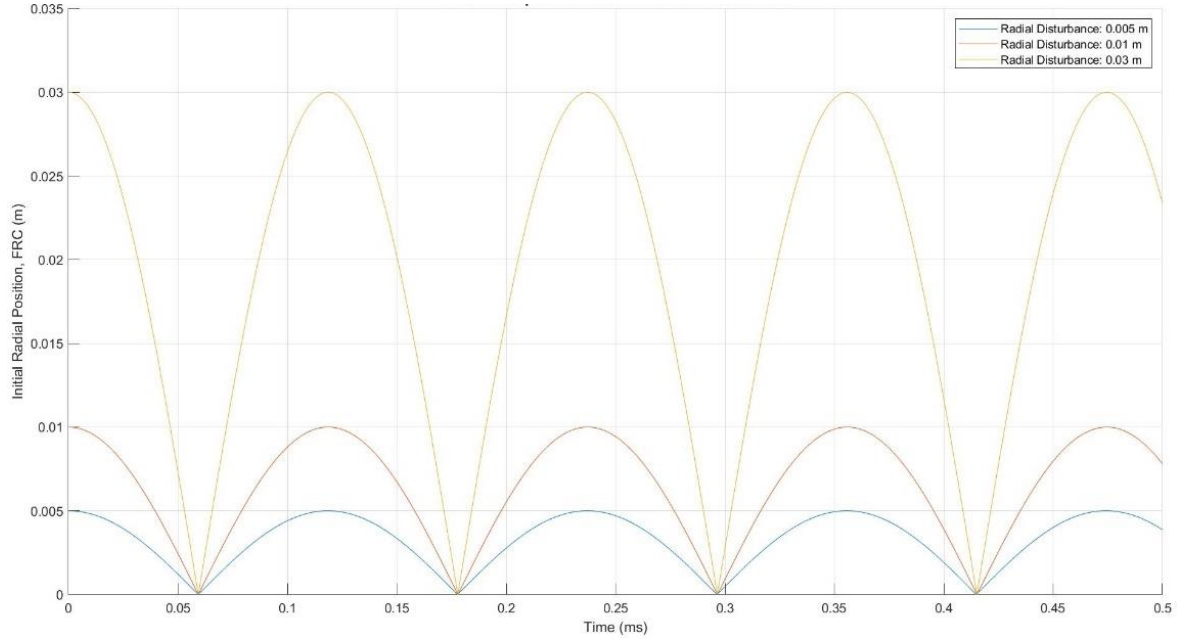

Figure 18. FRC Plasma Response to Radial Perturbation in Vacuum Magnetic Field

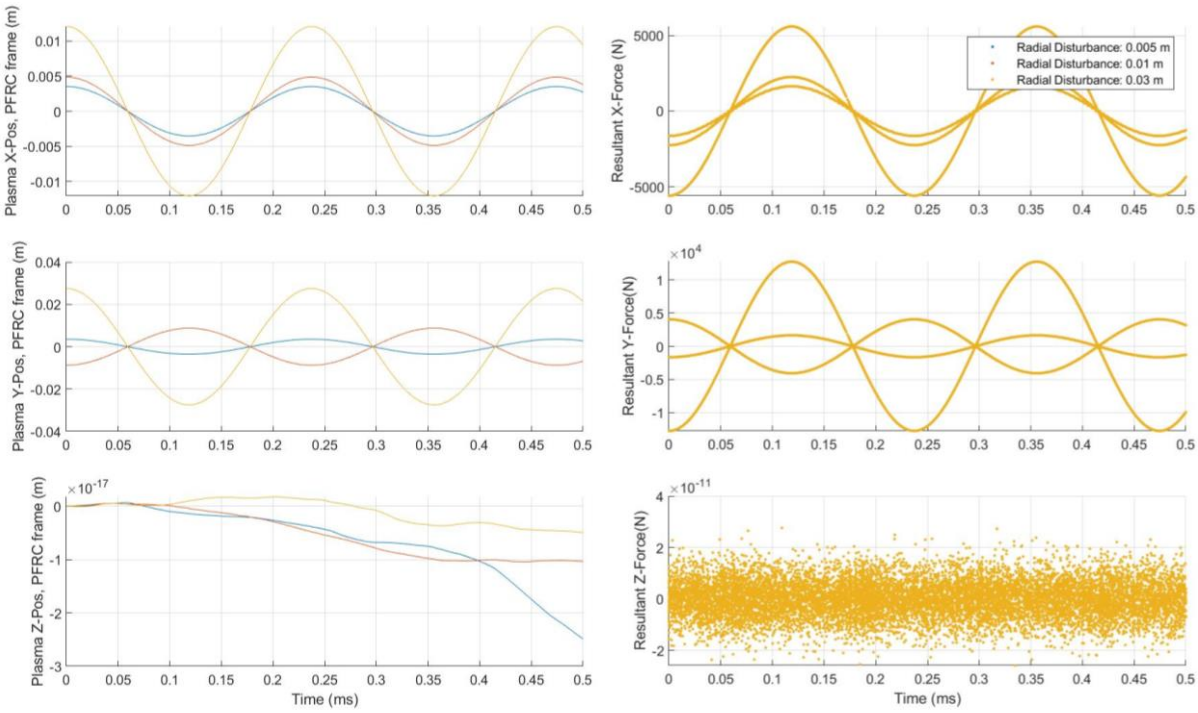

Figure 19. FRC Plasma Response to Radial Perturbation in Vacuum Magnetic Field

The net force acting on the FRC plasma centroid ($\vec{F}_{CEN}$) is calculated as a function of radial perturbation in Figure 20, where negative radial force acts toward the origin. It is clear the net force driving FRC radial response varies linearly with radial perturbation. One should be able to analytically derive this linear result through systems analysis and is captured as future work under Chapter 7, activity 3.

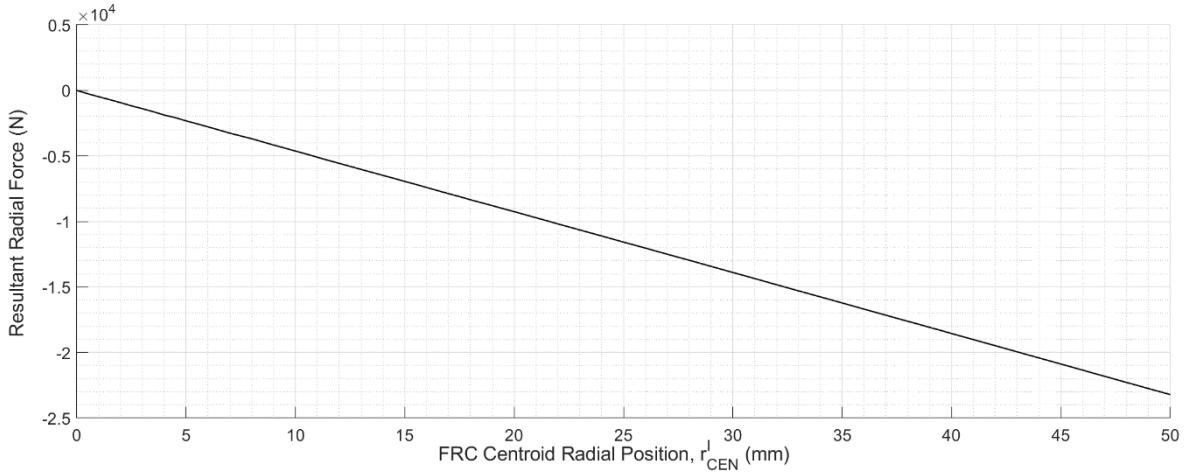

Figure 20. Resultant Force due to radial position of FRC Plasma in Vacuum Magnetic Field

5.4 Result 2: Plasma Response to Axial Perturbation (Constant Current EM Coils)

The FRC centroid position response to *axial perturbations* is shown in Figure 21. The FRC is demonstrated to be axially driven away from the origin (Subplot 3 *"Plasma Z-Pos"*) until solver termination conditions are exercised, "exceeding z-axis boundary", indicating FRC plasma is unstable axially. Note, the plasma experiences significant restoring forces as it approaches the nozzle coils (at around $\left|z_{\mathrm{CEN}}^{l}\right| > 1.25\mathrm{m}$). As shown at ~5.5E-4 ms onwards, the plasma slows down, however, had clearly gained significant momentum, and does not come to rest before hitting termination conditions. Discussed further in Figure 23 below.

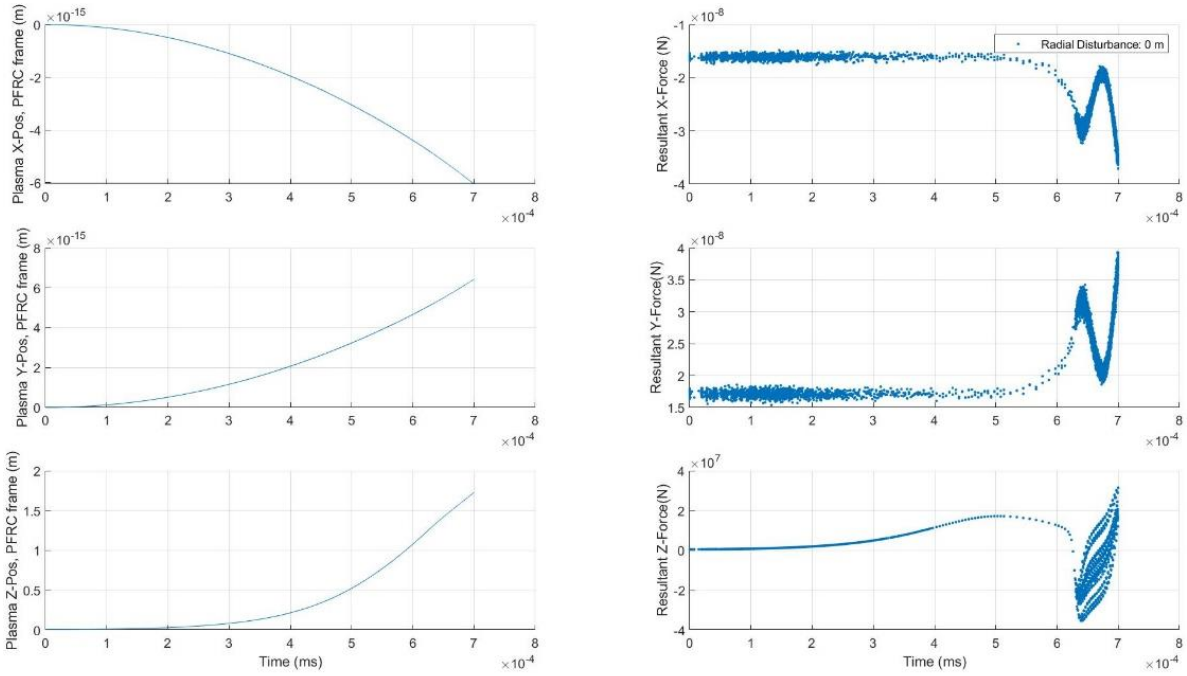

Figure 21. FRC Plasma Response to Axial Perturbation in Vacuum Magnetic Field

The FRC radial position is shown in Figure 22 to grow exponentially, however, on the order of 1×10^{-15}m and is likely due to plasma discretisation (differential volume element significantly larger than scale of radial displacement) and numerical precision. No simulation runs for axial perturbations have been able to demonstrate unstable growth in FRC radial position, solver termination conditions are always exercised (due to unstable response in axial position) before FRC radial position can achieve a drift beyond 1×10^{-14}m.

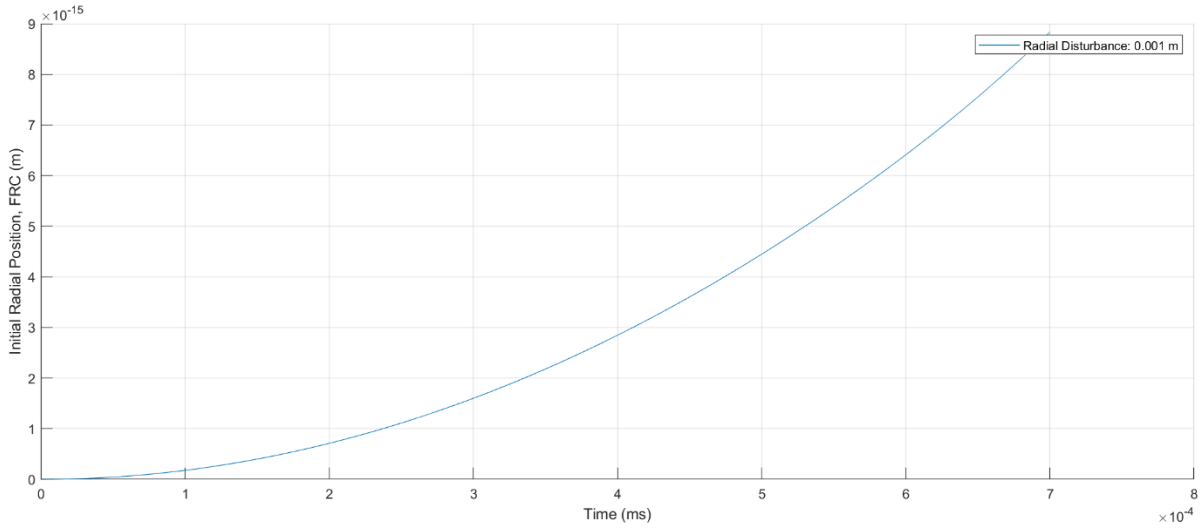

Figure 22. FRC Plasma Response to Axial Perturbation in Vacuum Magnetic Field

The net axial force acting on the FRC plasma centroid ($\vec{F}_{CEN,z}$) is given as a function of axial perturbation in Figure 23. The axial force is clearly destabilising when the FRC centroid position is within the region: $0\text{m} < \left|z^{I}_{\text{CEN}}\right| < 1.25\text{m}$, whilst axial force is 0N at the origin. Note: the fluctuations shown over the nozzle coils at ±1.5m is an artifact of the solver, and due to plasma discretisation and its physical intersection with coil actuators at the ends (solver neglects physical contact between objects). Solver is deemed applicable z^{I}<1.25m from origin.

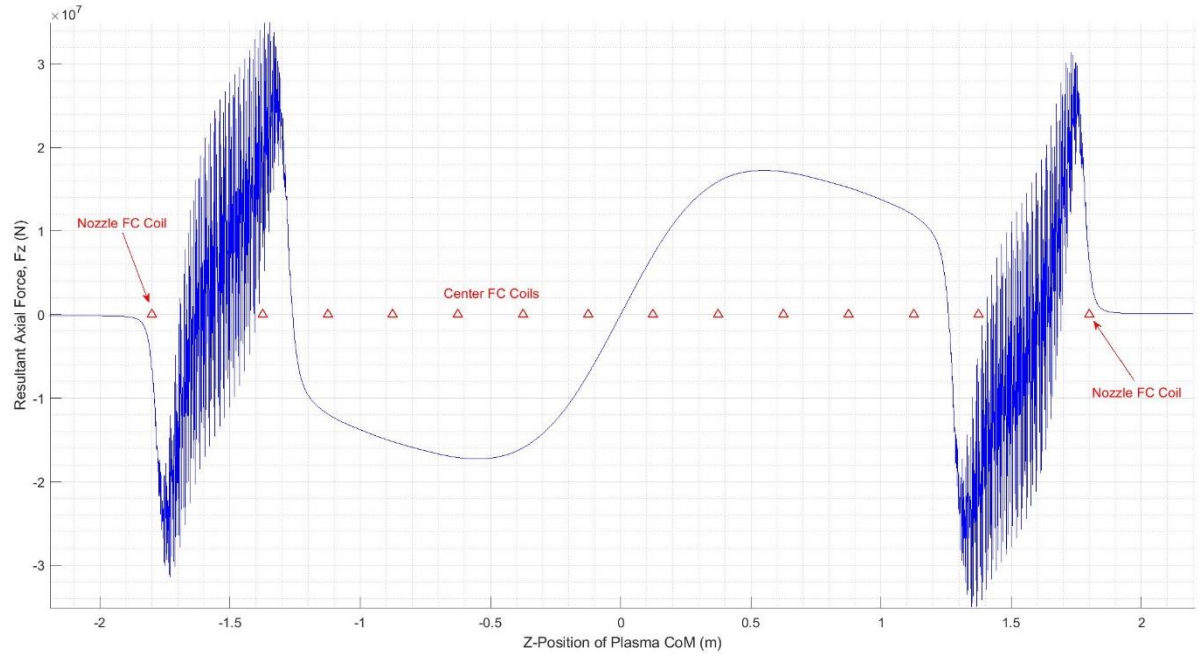

Figure 23. Resultant Axial Force due to Axial Perturbation in Vacuum Magnetic Field

Additionally, shown in Figure 23 nozzle coils produce significant restoring forces (±3E7 N) when the FRC position approaches $z^I_{\mathrm{CEN}} \cong \pm 1.3\mathrm{m}$ (consider a smooth-fitting curve at through fluctuations). This nozzle restoring force is demonstrated in Figure 24 for an oblate FRC (small FRC that can fit) initialised at $z^I_{\mathrm{CEN}} = 1.3\mathrm{m}$, in-front of a nozzle coil. The FRC plasma exhibits undamped oscillation axially about a null point ~1.25m (see Subplot: *"Plasma Z-Pos"*). The nozzle coil clearly restores the plasma axially toward the origin, while axial field coils drive the plasma away from the origin, potentially resulting in formation of an equilibrium point at $z^I \cong 1.25\mathrm{m}$ for the given coil configuration.

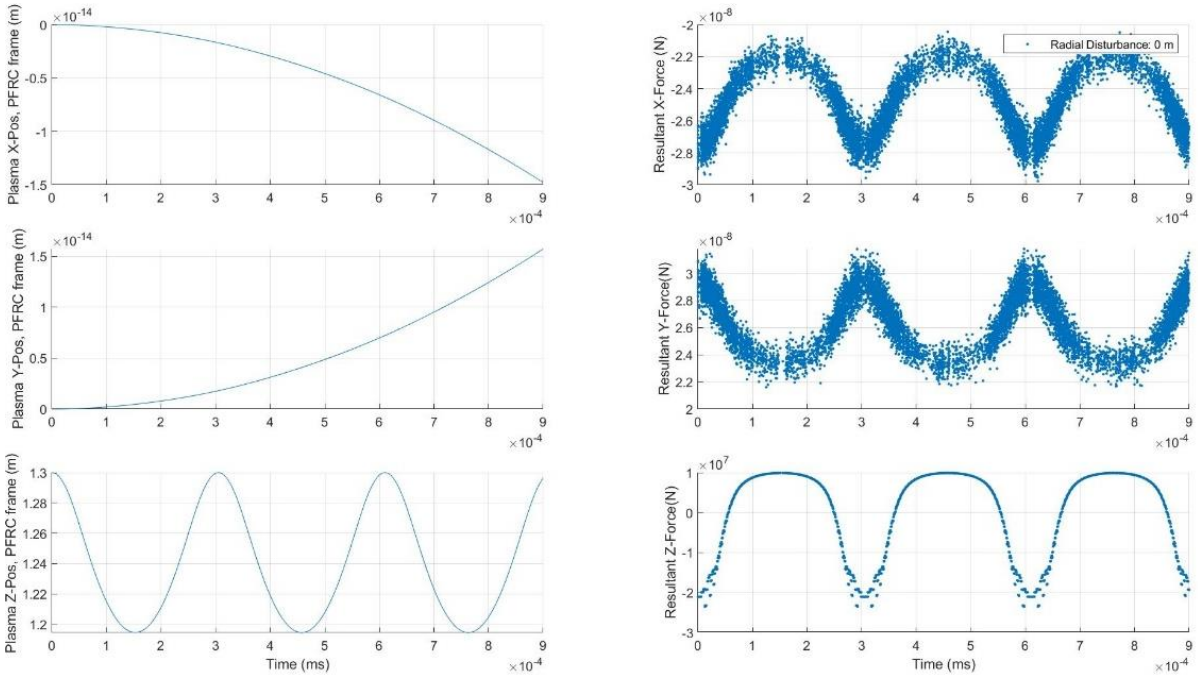

Figure 24. FRC Plasma Response to Nozzle Coil in Vacuum Magnetic Field

5.5 Result 3: Plasma Response with Flux Conservers (Superconducting Coils)

5.5.1 Radial Perturbations

With superconducting coil actuators, the FRC position response to *radial perturbation* produces similar results to constant-current EM coils (i.e. exhibits constant-frequency undamped oscillations in radial position about the origin, similar to that shown in Figure 19).

This is expected, since no variation in the external magnetic field (flux-conserving currents/fields or vacuum field) should occur as there is negligible change in FRC axial position over time, per Table 3. The flux-conserving currents induced in $N = 12$ superconducting coils and subsequent flux-conserving field experienced by the plasma are shown to remain fairly constant while FRC is radially oscillating in Figure 26.

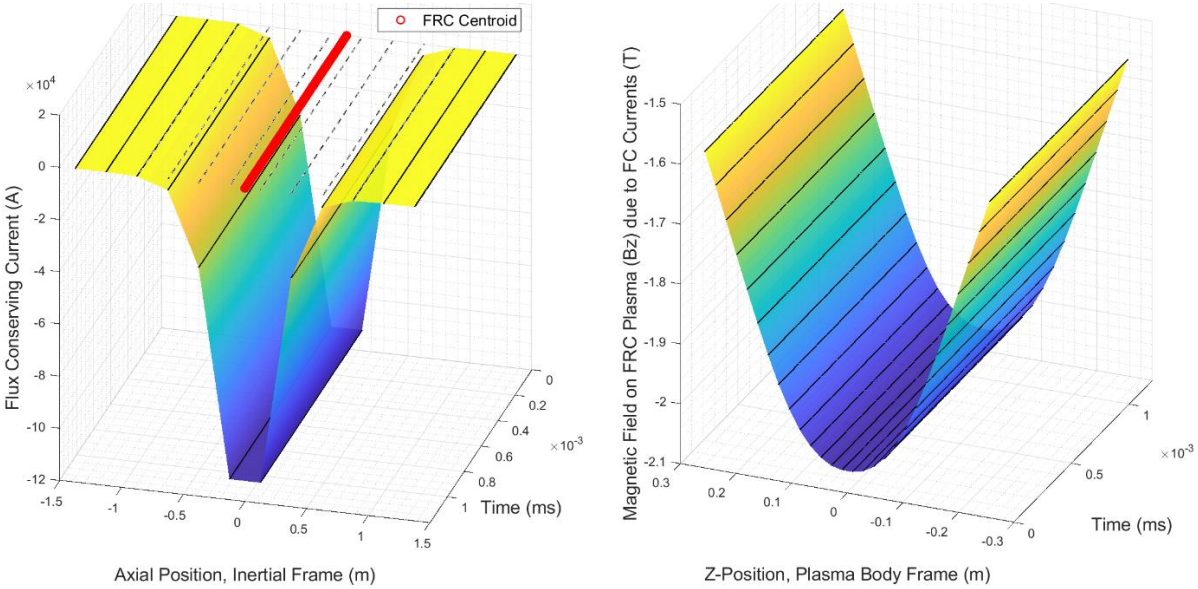

Figure 25. FRC Position Response to Radial Perturbation, a) Flux-Conserving Current, b) Flux-Conserving Field Acting on FRC Plasma

5.5.2 Axial Perturbations

With superconducting coil actuators, the FRC position response to *axial perturbations* produces similar results to constant-current EM coils (i.e. FRC is axially driven away from the origin until solver termination conditions are exercised, "exceeding z-axis boundary", per Figure 21). **N.B.** This is certainly not the response expected per Table 2 for flux-conserving coils (to be similar as constant-current EM coils), further investigation is required. Note however, flux-conserving currents are successfully induced in $N = 12$ superconducting coils as the FRC plasma transits through the device as demonstrated in Figure 27, and values for simulated variables shown in Table 8 were cross-referenced as a sanity-check.

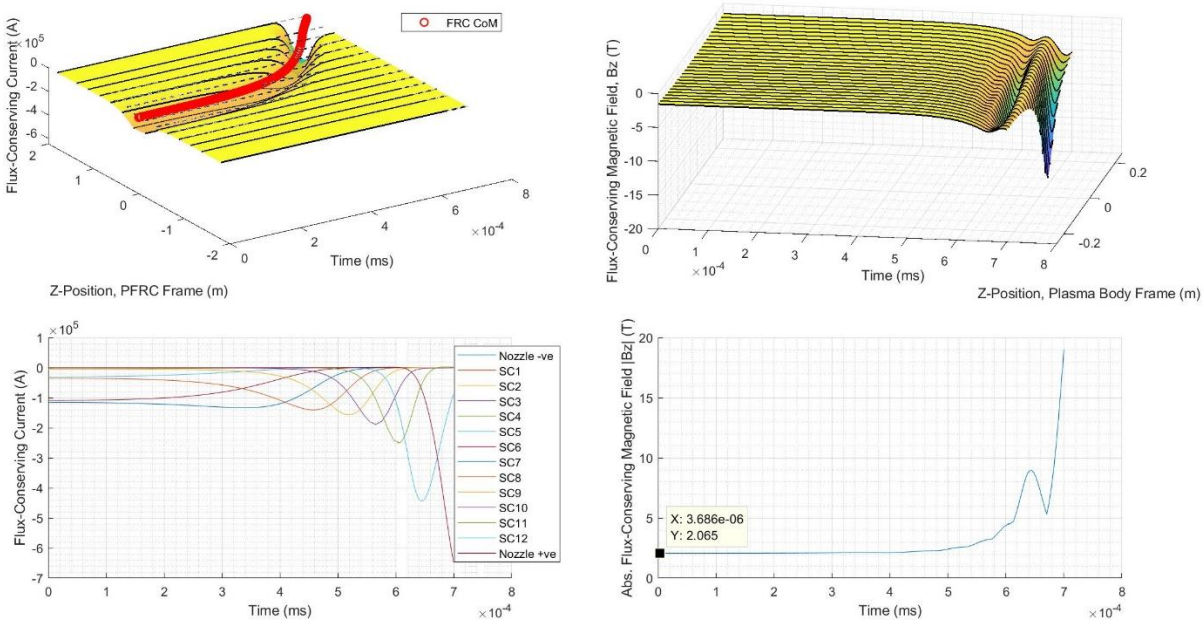

Figure 26. FRC Plasma Response to Axial Perturbation with Flux Conserving Field

A case not listed as criteria in Table 2 is presented here out of interest. The reversal of cases 1 and 2 (FRC axially stable, radially unstable) is one other possibility theorised [8]. This case is demonstrated in Figure 27, where for *axial perturbations* FRC axial position is shown to exhibit undamped oscillations about the origin, axially bounded response, while for *radial perturbations* (not shown) FRC is confirmed to be driven away from the origin radially, thus radially unstable. This case is excluded as it does not conform to the DFD/PFRC configuration (either plasma current direction or magnetic field direction must be reversed).

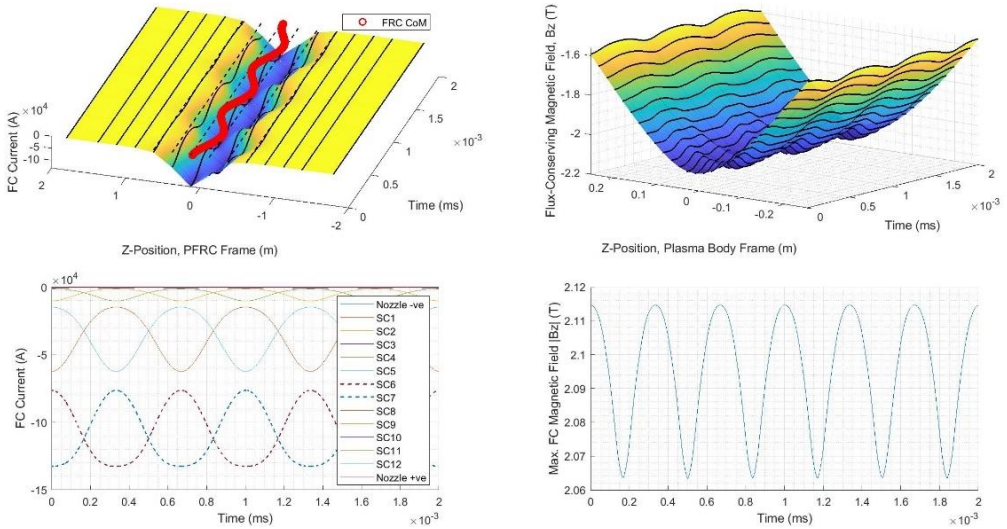

Figure 27. FRC Plasma Response to Axial Perturbation with Flux Conserving Field

5.6 Verification of Numerical Results

Numerical results are verified qualitatively against Table 2, with outcomes summarised in Table 7. The FRC centroid position response is consistent for cases involving constant-current copper EM coils (cases 1 and 2), however, further work is required for cases involving superconducting/flux-conserving coils (case 3), including a thorough review of the solver captured as future work under Chapter 7.1.b.

Table 7. Numerical Results Evaluated against Criteria

Case	Perturbation	Actuator Coil	Expected Plasma Response	Result
1	**Radial** perturbation to FRC centroid position	Copper EM Axisymmetric **Constant Current**	*Stable* or *bounded* open-loop response in axial and radial position (for $B_{v_z} < 0$)	**PASS** (Consistent with Sim)
2	**Axal** perturbation to FRC centroid position	Copper EM Axisymmetric **Constant Current**	*Unstable* or *unbounded* open-loop response in axial position (for $B_{v_z} < 0$)	**PASS** (Consistent with Sim)
3	**3DOF** perturbation to FRC centroid position	Superconductor Axisymmetric **Flux-conserving Current**	Unknown. Expecting *stable/bounded* radial and axial position response. Expecting plasma position to be "locked" relative to SC coils (plasma flux completely counteracted by SC coils, hence resisting changes in FRC position)	**Further Work Required**

Chapter 6. Conclusions

A mathematical model was derived for the FRC plasma translational dynamics, subject to coaxial superconducting coil actuators and constant-current copper coil actuators. One term of the model remains not in closed-form, specifically elliptic integrals in expressions for mutual inductance. A numerical solver was developed in MATLAB using the derived model, providing a tool for FRC centroid position control design and analysis (for example, aiding in the analysis of coil actuator configurations, including more complex coil geometries or confinement schemes such as saddle coils). The current solver may be extended to factor FRC rotational kinematics, captured as future work under Chapter 7.6.

Simulations were run verifying the FRC position exhibited a response consistent with expectations for constant-current copper EM coils. For radial perturbations, FRC response is demonstrated to be radially bounded (constant-frequency undamped radial-oscillation about the origin). For axial perturbations, FRC has an axially unstable response (driven away from the origin axially, exceeding physical limits). For cases involving superconducting coils (flux-conservers), the FRC centroid position did not exhibit a response consistent with expectations. Flux-conserving currents are successfully modelled and simulated as a function of FRC centroid position. However, for axial perturbations, FRC response is axially unstable (driven away from the origin axially), further work is required here as this is contrary to our expectation/hypothesis that the FRC plasma axial position should be “locked” relative to flux-conserving coils or axial motion entirely resisted.

Chapter 7. Future Work

The following activities benefit FRC plasma stability analysis and control design the most given work conducted in this master's thesis:

1. Potential to Publish:

   At current, potential exists for two publications on rigid-body modelling of FRC plasmas (for stability and control analysis) and the numerical results, specifically:

   a. FRC centroid position response to *radial* and *axial perturbations* given constant-current coaxial electromagnet coil actuators (reporting on the model/findings for cases 1 and 2 in Table 2). Non flux conserving.

   b. FRC centroid position response to *radial* and *axial perturbations* given flux-conserving superconducting coils (reporting on model/findings for case 3 in Table 2). However, this requires more rigorous review of solver source code than has been applied in this master's thesis and a more detailed assessment of values in Table 8 with PSS.

2. Mutual Inductance Analytical-Form:

   At current, mutual inductance given by Equation (43) is not in closed form (analytical form). Elliptic integrals may be approximated effectively through methods in [19] to derive closed form expressions. Some effort could be spent approximating elliptic integrals for some perturbation about the PFRC origin Figure 17 (if unable to express globally) or that which is deemed sufficient to PFRC operating conditions.

3. Systems Analysis and Control Design:

Apply dynamical system analysis and control techniques to the model derived in Table 4 (e.g. stability analysis, observability, controllability/reachability, OL/CL control). Should ideally include flux-conserving currents $\vec{I}_C$ from Equation (51) in state vector given by Equation (56). Requires closed-form mutual inductance. Currently, this is the only term for FRC centroid position in non-closed form.

4. Investigate Actuator Configurations:

   At current, can begin investigating different axisymmetric actuator coil configurations, and passive/active control schemes (EM coil currents), with little to no changes required to the solver.

5. Modelling Complex Actuator Circuits:

   More complex actuator geometries (such as *saddle coils* / non-axisymmetric coils for stabilisation/control of higher plasma modes, per Section 1.2.2.2.b) require replacing Maxwell Coil assumptions with Biot-savart Law in Equation (48) to solve a full 3D magnetic field (rather than assuming axisymmetric coils).

6. Stabilisation of Higher FRC Plasma Modes:

   Eventually, it is desired to stabilise and control higher plasma mode numbers such as plasma tilt mode (m=1, n=1) and radial elongation mode (m=2). However, FRC centroid position control should come first. For higher modes, need to factor FRC rigid-body rotations, specifically for tilt-mode, due to Lorentz force torques and gyro-viscous forces exerted on the FRC plasma per [16]. Whereby, ions are assumed to carry most of the plasma momentum, causing inherent plasma rotation due to ion diamagnetic drift [6].

Appendix

Vector Calculus in Cylindrical Coordinate System

The Cylindrical Coordinate System is illustrated in Figure 28. Unit vectors $\hat{e}_r, \hat{e}_\phi, \hat{e}_z$ define the radial, azimuth and axial directions respectively for a differential element.

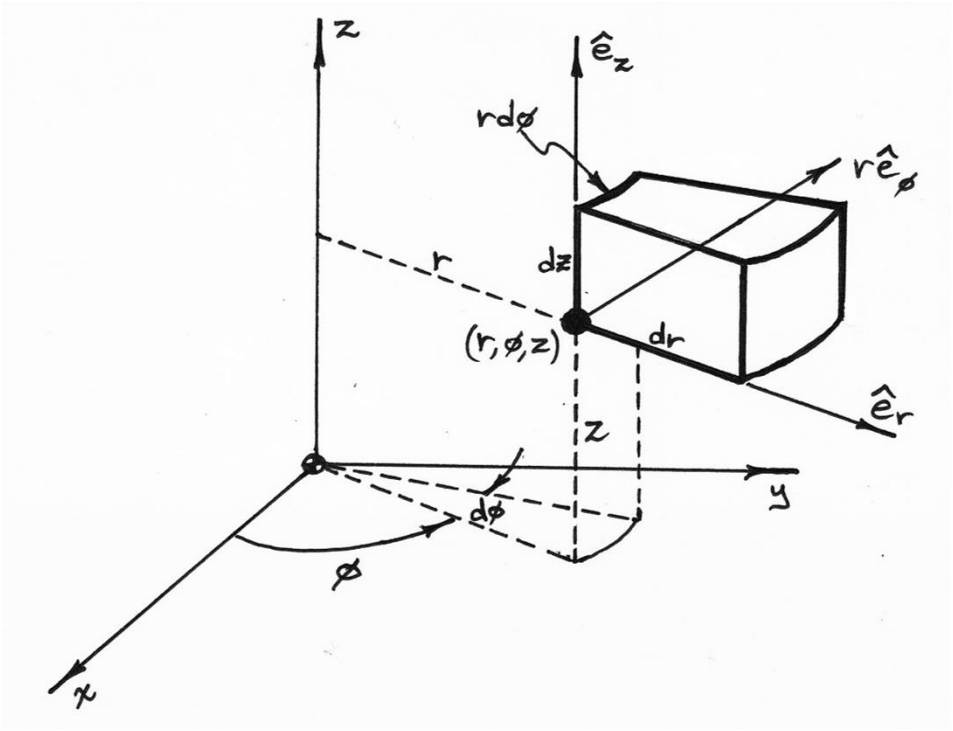

Figure 28. Differential Element in Cylindrical Coordinate System

Differential Volume in cylindrical coordinates:

$$dV = dr(rd\phi)dz = r\,dr\,d\phi\,dz \tag{66}$$

Vector Field in cylindrical coordinates:

$$\vec{A} = A_r\hat{e}_r + A_\phi\hat{e}_\phi + A_z\hat{e}_z \tag{67}$$

Divergence of vector field in cylindrical coordinates:

$$\nabla \cdot \vec{A} = \frac{1}{r}\frac{\partial(rA_r)}{\partial r} + \frac{1}{r}\frac{\partial A_\phi}{\partial \phi} + \frac{\partial A_z}{\partial z} \tag{68}$$

Curl of vector field in cylindrical coordinates:

$$\nabla \times \vec{A} = \frac{1}{r}\begin{vmatrix} \hat{e}_r & r\hat{e}_\phi & \hat{e}_z \\ \frac{\partial}{\partial r} & \frac{\partial}{\partial \phi} & \frac{\partial}{\partial z} \\ A_r & rA_\phi & A_z \end{vmatrix}$$

$$\nabla \times \vec{A} = \left(\frac{1}{r}\frac{\partial A_z}{\partial \phi} - \frac{\partial A_\phi}{\partial z}\right)\hat{e}_r + \left(\frac{\partial A_r}{\partial z} - \frac{\partial A_z}{\partial r}\right)\hat{e}_\phi + \frac{1}{r}\left(\frac{\partial (rA_\phi)}{\partial r} - \frac{\partial A_r}{\partial \phi}\right)\hat{e}_z \qquad (69)$$

Quantities of Simulated Variables (Solver Quality Check)

Quantities for certain model variables are recorded in Table 8 for the purpose of a quick quality/consistency check of the solver with PSS. Ideally a more thorough review of the solver is required and captured as future work under Chapter 7, activity 1.b.

Table 8. Orders of Magnitude of Model Variables Simulated

Variable	Numerical Value
FC Current in Superconductor Coils	10e4 to 15e4 A
FC Magnetic Flux sensed at the FRC (max.)	0.04 Wb
FC Magnetic Field sensed at the FRC	1-2 T
FRC Plasma Current (max.)	600 A
Resulting Force on FRC Centroid	1e5 N ($F_{\mathrm{CEN},r}$), 5e6 N ($F_{\mathrm{CEN,z}}$)
Period of radial and axial oscillation	1e-6 sec (0.001 ms)

Acronyms and Abbreviations

DFD	Direct Fusion Drive
EM	Electromagnetic
FC	Flux Conserving
FRC	Field-Reversed Configuration
LCFS	Last Closed Flux Surface
MHD	Magnetohydrodynamic
PFRC	Princeton Field-Reversed Configuration
PPPL	Princeton Plasma Physics Laboratory
PSS	Princeton Satellite Systems
RRM	Rigid-Rotor Model
SC	Superconducting

Overview of Numerical Solver MATLAB Scripts

An outline of the MATLAB scripts developed for the numerical Solver (FRC plasma position response) is given in Figure 29. A description for each script is provided in Table 9.

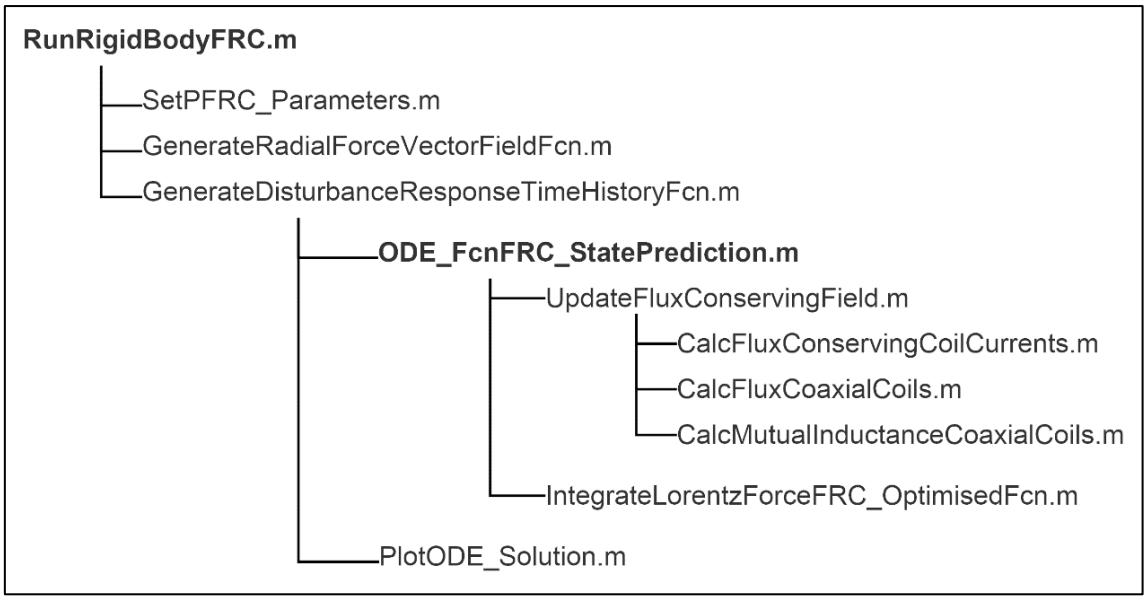

Figure 29. Overview of MATLAB Scripts used in Rigid-Body FRC Solver

Table 9. Description of MATLAB Scripts used in Rigid-Body FRC Solver

Filename	Description
RunRigidBodyFRC.m	Main function (entry point).
SetPFRC_Parameters.m	- Plasma / DFD Parameters per Table 5 and Table 6. - Discretisation of plasma body (plasma coils, plasma volume elements) per Figure 14. - Solver Settings.
GenerateDisturbanceResponseTimeHistoryFcn.m	Simulate plasma 3DOF translational response to axial and radial perturbations from origin.
ODE_FcnFRC_StatePrediction.m	ODE function (for ODE113 solver).
ODE_InterruptEvents.m	Solver Termination Conditions (r^I, z^I machine limits)
IntegrateLorentzForceFRC_OptimisedFcn.m	Integrates Lorentz forces per Equation (58) using param. discretised plasma.
IntegrateLorentzForceFRC_Fcn.m	Integrates Lorentz forces per Equation (58) using online plasma discretisation.
UpdateFluxConservingField.m	Calculate magnetic flux through the plasma due to flux-conserving currents, per Equation (52).

Table 9. Description of MATLAB Scripts used in Rigid-Body FRC Solver, Continued

Filename	Description
CalcFluxConservingCoilCurrents.m	Calculate flux-conserving current due to plasma flux, per Equations (47) to (51).
CalcFluxCoaxialCoils.m	Calculate magnetic flux through coil-1 due to coil-2.
CalcMutualInductanceCoaxialCoils.m	Calculate mutual inductance between two coils, per Equations (40) to (43).
PlotODE_Solution.m	Plot plasma kinematic response, resultant force, flux-conserving current
GenerateRadialForceVectorFieldFcn.m	Calculate only radial forces on plasma given radial perturbations from origin.

References

[1] S. Thomas, “Direct Fusion Drive: Enabling Rapid Deep Space Propulsion,” in *Future In-Space Operations (FISO) Telecon Presentations,* 2019.

[2] H. Gota, M. Binderbauer, T. Tajima, S. Putvinski, M. Tuszewski and TAE Team, “C-2U and C-2W Field-Reversed Configuration Experiments,” in *Exploratory Plasma and Fusion Research Workshop,* Vancouver, British Columbia, Canada, 2017.

[3] L. C. Steinhauer, “Review of Field-Reversed Configurations,” *Physics of Plasmas,* vol. 18, no. 070501, 2011.

[4] S. Thomas, M. Paluszek and S. Cohen, “Fusion-Enabled Pluto Orbiter and Lander, NIAC Phase I Final Report,” NASA Award Number: NNX16AK28G, New Jersey, 2017.

[5] J. D. A. Mena, M. Lee, L. M. Evans and D. V. Griffiths, “THE STOCHASTIC FINITE ELEMENT METHOD FOR NUCLEAR APPLICATIONS,” in *European Congress on Computational Methods in Applied Sciences and Engineering (ECCOMAS) Congress VII*, Crete Island, Greece, 2016 .

[6] N. Iwasawa, A. Ishida and L. C. Steinhauer, “Linear Gyroviscous Stability of Field-Reversed COnfigurations with Static Equilibrium,” *Physics of Plasmas,* vol. 8, no. 4, pp. 1240-1247, 2001.

[7] S. Jeon, G. Jang, H. Choi and S. Park, “Magnetic Navigation System With Gradient and Uniform Saddle Coils for the Wireless Manipulation of Micro-Robots in Human Blood Vessels,” *IEEE Transactions on Magnetics ,* vol. 46, no. 6, pp. 1943-1946, 2010.

[8] N. Rath, M. Onofri and D. C. Barnes, “Positional stability of field-reversed-configurations in the presence of resistive walls,” *Physics of Plasmas,* vol. 23, no. 064505, pp. 1-3, 2016.

[9] N. Rath, M. Onofri, S. A. Dettrick, D. C. Barnes and J. Romero, “Modeling feedback control of unstable separatrix location in beam-driven field-reversed configurations,” *Physics of Plasmas,* vol. 24, no. 042504, pp. 1-14, 2017.

[10] A. R. Bell, “Computational Simulations of Plasma,” *Astrophysics and Space Science,* vol. 256, pp. 13-35, 1997.

[11] S. A. Cohen, C. Swanson, N. Mcgreivy, A. Raja, E. Evans, P. Jandovitz, M. Khodak, G. Pajer, T. D. Rognlien, S. Thomas and M. Paluszek, “Direct Fusion Drive for Interstellar Exploration,” *Journal of the British Interplanetary Society,* vol. 72, no. 2, pp. 37-50, 2019.

[12] L. Scibile, “Non-linear Control of the Plasma Vertical Position in a Tokamak,” University of Oxford, Abingdon, UK, 1997.

[13] R. Kanno, A. Ishida and L. C. Steinhauer, “Ideal-Magnetohydrodynamic-Stable Tilting in Field-Reversed Configurations,” *Journal of the Physical Society of Japan,* vol. 64, no. 2, pp. 463-478, 1995.

[14] R. G. Storer, “Compact Torus Equilibria Set up in the Rotamak by Rotating Magnetic Fields,” *Nuclear Instruments and Methods,* no. 207, pp. 135-138, 1983.

[15] I. J. Donnelly, E. K. Rose and J. L. Cook, “Magnetohydrodynamic Equillibrium Models for Rotamak Plasmas,” *Australian Journal of Physics,* vol. 40, pp. 175-183, 1987.

[16] H. Ji, M. Yamada, R. Kulsrud, N. Pomphrey and H. Himura, “Studies of global stability of field-reversed configuration plasmas using a rigid body model,” *Physics of Plasmas,* pp. Volume 5, Number 10, 1998.

[17] C. Akyel and S. I. Babic, “Mutual Inductance Between Coaxial Circular Coils of Rectangular Cross Section and Thin Coaxial Circular Coils with Constant Current Density in Air (Filament Method),” *WSEAS International Conference on Applications of Electrical Engineering,* vol. 6, pp. 102-108, 2007.

[18] M. Paluszek, “PFRC Dynamics and Control (Internal Memo),” Princeton Satellite Systems, New Jersey, January 2020.

[19] E. B. Rosa and L. Cohen, “The Mutual Inductance of Two Circular Coaxial Coils of Rectangular Section,” *Department of Commerce Bulletin of the Bureau of Standards,* vol. 2, no. 3, pp. 359-414, 2018.

[20] T. Kanki, S. Okada and S. Goto, “Magnetohydrodynamic Simulation of Dynamic Behaviour of a Field-Reversed Configuration During Magnetic Mirror Reflection,” *Physics of Plasmas,* vol. 10, no. 9, pp. 3635-3643, 2003.